



---

1 **Measurement and model analyses of the ozone variation during 2006 to 2015 and its response**  
2 **to emission change in megacity Shanghai, China**

3

4 Jianming Xu<sup>1,2</sup>, Xuexi Tie<sup>3,4</sup>, Wei Gao<sup>1,2</sup>, Yanfen Lin<sup>5</sup>, and Qingyan Fu<sup>5</sup>

5

6 <sup>1</sup> Yangtze River Delta Center for Environmental Meteorology Prediction and Warning, Shanghai  
7 Meteorological Service, Shanghai, 200135, China

8 <sup>2</sup> Shanghai Key Laboratory of Health and Meteorology, Shanghai Meteorological Service, Shanghai,  
9 200135, China

10 <sup>3</sup> Key Laboratory of Aerosol Chemistry & Physics, SKLLQG, Institute of Earth Environment, Chinese  
11 Academy of Science, Xi'an, 710061, China

12 <sup>4</sup> Center for Excellence in Urban Atmospheric Environment, Institute of Urban Environment,  
13 Chinese Academy of Science, Xiamen, 361021, China

14 <sup>5</sup> Shanghai Environmental Monitoring Center, Shanghai, 200135, China

15

16

17

18

19 Correspondence: Xuexi Tie (tiexx@ieecas.cn)

20



21       **Abstract.** The fine particles (PM<sub>2.5</sub>) in China decrease significantly in recent years as a result  
22 of the implement of Chinese Clean Air Action Plan since 2013, while the O<sub>3</sub> pollution is getting  
23 worse, especially in megacities such as Beijing and Shanghai. Better understanding the elevated  
24 O<sub>3</sub> pollution in Chinese megacities and its response to emission change is important for  
25 developing an effective emission control strategy in future. In this study, we analyze the  
26 significant increasing trend of O<sub>3</sub> concentration from 2006 to 2015 in the megacity Shanghai with  
27 the variability of 1-1.3 ppbv yr<sup>-1</sup>. It is likely attributed to the notable reduction of NO<sub>x</sub>  
28 concentration with the decreasing rate of 1.86-2.15 ppbv yr<sup>-1</sup> accompanied with the little change  
29 of VOCs during the same period excluding the weak trends of meteorological impacts on local  
30 dispersion (wind speed), regional transport (wind direction) and O<sub>3</sub> photolysis (solar radiation). It  
31 is further illustrated by using a state of the art regional chemical/dynamical model (WRF-Chem)  
32 to explore the O<sub>3</sub> variation response to the reduction of NO<sub>x</sub> emission in Shanghai. The control  
33 experiment conducted in September of 2009 shows very excellent performance for O<sub>3</sub> and NO<sub>x</sub>  
34 simulations including both the spatial distribution pattern, and the day by day variation by  
35 comparing with 6 in-situ measurements from MIRAGE-shanghai field campaign. Sensitive  
36 experiments with 30% reduction of NO<sub>x</sub> emission from 2009 to 2015 in Shanghai estimated by  
37 Shanghai Environmental Monitoring Center shows that the calculated O<sub>3</sub> concentrations exhibit  
38 obvious enhancement by 4-7 ppbv in urban zones with the increasing variability of 0.96-1.06  
39 ppbv yr<sup>-1</sup>, which is well consistent with the observed O<sub>3</sub> trend as a result of the strong  
40 VOC-limited condition for O<sub>3</sub> production. The large reduction of NO<sub>x</sub> combined with less change  
41 of VOCs during the past ten years promotes the O<sub>3</sub> production in Shanghai to move towards  
42 NO<sub>x</sub>-limited regime. Further analysis of WRF-Chem experiments and O<sub>3</sub> isopleths diagram  
43 suggests that the O<sub>3</sub> production in downtown is still under VOC-limited regime after 2015 despite  
44 of the remarkable NO<sub>x</sub> reduction, while moves to the transition regime between NO<sub>x</sub>-limited and  
45 VOC-limited in sub-urban zones. Supposing the insignificant VOCs variation persists, the O<sub>3</sub>  
46 concentration in downtown would keep increasing till 2020 with the further 20% reduction of  
47 NO<sub>x</sub> emission after 2015 estimated by Shanghai Clean Air Action Plan. While there are less O<sub>3</sub>  
48 change in other regions where the O<sub>3</sub> production is not under VOC-limited regime. The O<sub>3</sub>  
49 production in Shanghai will switch from VOC-limited to NO<sub>x</sub>-limited regime after 2020 except  
50 downtown area which is likely close to the transition regime. As a result the O<sub>3</sub> concentration will  
51 decrease by 2-3 ppbv in sub-urban zones, and more than 4 ppbv in suburb response to 20%  
52 reduction of NO<sub>x</sub> emission after 2020, whereas is not sensitive to both NO<sub>x</sub> and VOCs changes in  
53 downtown. This result reveals that the control strategy of O<sub>3</sub> pollution is a very complex process,  
54 and needs to be carefully studied.

55

56       **Key Words:** O<sub>3</sub> pollution in Shanghai, Long-term O<sub>3</sub> trend, WRF-Chem

57



---

## 58 1 Introduction

59 Ozone ( $O_3$ ) in the troposphere plays the important role in the oxidation of chemically and  
60 climatically relevant trace gases, hence regulating their lifetime in the atmosphere (Monks et al.,  
61 2015). In the lower troposphere,  $O_3$  is produced from photochemical reactions involving volatile  
62 organic compounds (VOCs, broadly including CO) and nitrogen oxides ( $NO_x = NO + NO_2$ ) in the  
63 presence of sunlight (Brasseur et al., 1999). As a strong oxidant,  $O_3$  at ground level is detrimental  
64 to human health and vegetation (Tai et al., 2014), and has been received continuous attention  
65 from both the scientific and regulatory communities in the past three decades.

66 Shanghai has emerged as one of the largest megacities in the world over the last two  
67 decades. The city has a fleet of over 3.6 million vehicles and the population of over 2400 million  
68 permanent residents, which results in high emissions of  $NO_x$ , VOCs, and primary particulate  
69 matter (PM) to the atmosphere from industrial and commercial activities, leading to the  
70 photochemical smog formation. Persistent high level of surface  $O_3$  and PM were observed in  
71 Shanghai during the past ten years (Geng et al., 2007; Ran et al., 2009; Tie et al., 2009a; Xu et al.,  
72 2015). In order to mitigate the adverse impacts from severe air pollution, the Clean Air Action  
73 Plan was issued in the end of 2013 to implement the emission reduction program in Shanghai  
74 and its neighboring area. As a result, the annual mean  $PM_{2.5}$  (particles with diameter  $\leq 2.5 \mu m$ )  
75 mass concentration has decreased from  $50 \mu g m^{-3}$  in 2013 to  $39 \mu g m^{-3}$  in 2017. However  $O_3$   
76 pollution has been continuously worsen, with the non-attainment days increased from 99 d in  
77 2014 to 129 d in 2016. As a result,  $O_3$  becomes the primary air pollutant affecting the ambient air  
78 quality instead of  $PM_{2.5}$  in Shanghai. Similar issue has also been occurred in other cities in the  
79 eastern China (Lu et al., 2018). For example, the mean  $PM_{2.5}$  mass concentration over the 74  
80 major cities decreased by 40% from 2013 to 2017, whereas the maximum daily 8-h average  $O_3$   
81 concentration in summer exceeds the Chinese National Ambient Air Quality Standard over most of  
82 eastern China (Li et al., 2019). Thus better understanding the causes of elevated  $O_3$  in China is  
83 important for developing effective  $O_3$  control strategies, especially in megacities such as  
84 Shanghai.

85 A prerequisite to an effective emission-based  $O_3$  control strategy is to understand the  
86 temporal and spatial relationship between  $O_3$  and its precursors, and the response of  $O_3$   
87 concentrations to the changes in emissions of  $O_3$ -precursors (such as  $NO_x$  and VOCs, Lin et al.,  
88 1988). The relationship of  $O_3$  and  $O_3$ -precursors can be clarified as  $NO_x$ -limited or VOC-limited  
89 chemistry of  $O_3$  formation, which is usually defined based on the relative impact of a given  
90 percent reduction in  $NO_x$  relative to VOCs in the context of urban chemistry (Sillman, 1999).

91 Some observational and modeling works on  $O_3$  chemical formation and transformation have  
92 been carried out in Shanghai since 2007. The  $O_3$  production in Shanghai city is clearly under  
93 VOC-limited regime (Geng et al., 2007), in which the aromatics and alkenes play the dominant  
94 roles (Geng et al., 2008a). The aircraft measurements in Yangtze River Delta (YRD) region show  
95 the strong anti-correlation between  $NO_x$  and  $O_3$ , indicating the similar VOC-limited regime for  $O_3$   
96 production in the area neighboring Shanghai (Geng et al., 2008b). Thus either  $NO_x$  reduction or  
97 VOCs growth is favorable for  $O_3$  enhancement in Shanghai. Gao et al. (2017) reported that  $O_3$   
98 concentration in Shanghai downtown increased 67% from 2006 to 2015, whereas  $NO_x$   
99 concentration decreased about 38%. This is also consistent with the results of Lin et al. (2017)  
100 that, the median of the maximum daily 8-h average  $O_3$  concentration in Shanghai increased  
101 notably from 2006 to 2016, with the rate of  $1.4 \text{ ppbv yr}^{-1}$ , while the  $NO_2$  decreased from 66.7 to



102 42.1  $\mu\text{g m}^{-3}$  with about 20% reduction. These previous studies provide the useful information  
103 regarding the  $\text{O}_3$  chemical formation and transformation in Shanghai. However, such  $\text{O}_3$  variation  
104 responding to emission change has not been clearly investigated. Considering that  $\text{O}_3$  formation  
105 is a complicated process including chemistry, transport, emission, deposition and their  
106 interactions, the chemical transport model is the powerful tool to gain an understanding of these  
107 interacting processes. For example, Lei et al. (2007), Ying et al. (2009) and Song et al. (2010)  
108 investigated the  $\text{O}_3$  production rate and its sensitivity to emission changes of  $\text{O}_3$  precursors by  
109 CAMx model in Mexico City Metropolitan Area (MCMA). Tie et al. (2013) analyzed the  
110 comprehensive data of the MIRAGE-Shanghai field campaign by WRF-Chem model, and  
111 quantified the threshold value by the emission ratio of  $\text{NO}_x/\text{VOCs}$  for switching from VOC-limited  
112 to  $\text{NO}_x$ -limited in Shanghai. Recently Li et al. (2019) suggested an important cause of the  
113 increasing  $\text{O}_3$  in North China Plain (NCP) during 2013 to 2017 as the significant decrease in  $\text{PM}_{2.5}$   
114 slowing down the sink of hydroperoxy radicals and thus speeding up the  $\text{O}_3$  production by  
115 GOES-CHEM model. However such implication for  $\text{O}_3$  trend is not pervasive in YRD and other  
116 regions. Moreover, the 5-year  $\text{O}_3$  records seem rather short to examine the inter-annual  
117 variability of  $\text{O}_3$  concentration. The GOES-CHEM experiment with 50 km resolution maybe is  
118 suitable for the  $\text{O}_3$  simulation at regional scale but is too coarse to resolve the local  $\text{O}_3$  budget at  
119 urban scale, such as Beijing or Shanghai. To our knowledge, there are no peer-reviewed modeling  
120 studies focus on the past long term  $\text{O}_3$  variations response to emission changes conducted in  
121 Shanghai. Thus this paper extends the study of Tie et al. (2013) and Gao et al. (2017) to further  
122 examine the inter-annual  $\text{O}_3$  variations from 2005 to 2016 by long term measurements of  $\text{O}_3$  and  
123 its precursors in Shanghai. The effects of emission changes on long term  $\text{O}_3$  variability are  
124 evaluated by WRF-Chem model with high resolution and compared with measurements. The shift  
125 of  $\text{O}_3$  photochemical regime relative to the variations of  $\text{NO}_x$  and VOCs concentrations in the past  
126 ten years is discussed by  $\text{O}_3$  isopleths diagram combined with WRF-Chem model to provide more  
127 insights into the  $\text{O}_3$  control strategy. Moreover, the future  $\text{O}_3$  levels and its possible chemical  
128 regime in Shanghai are also discussed according to the Shanghai Clean Air Action Plan.

129 The paper is constructed as follows. The measurements and models used for this study are  
130 described in Sect. 2. The analysis on the long-term in-situ measurements of  $\text{O}_3$  and its precursors,  
131 as well as the model sensitive experiments are presented and discussed in Sect. 3-6. The  
132 conclusion is summarized in Sect. 7.

133

## 134 **2 Measurements and models**

### 135 **2.1 Measurements**

136 The measurements of  $\text{O}_3$  and  $\text{NO}_x$  are collected from 6 sites (XJH, PD, JS, BS, SS, DT) over  
137 Shanghai under different influence of air pollutant emissions. The XJH site is located at the  
138 downtown of Shanghai, which is strongly influenced by emission of transportation. The PD site is  
139 located at the sub-urban area near a big park, which is influenced by the mixed emissions of  
140 transportation and residential. The JS site is located in the south of Shanghai with several large  
141 chemical industries. The BS site is located in the north of Shanghai with some big steel and power  
142 plants. The SS site is located at the top of the sole hill (100 m a.g.l) in Shanghai, which has minor  
143 effect from regional emissions, and is influenced by regional transport. The DT site is located at a  
144 remote island without anthropogenic activities. These  $\text{O}_3$  and  $\text{NO}_x$  measurements are used for



145 the evaluation on WRF-Chem performance. In addition, the VOCs are sampled at the downtown  
146 site XJH and the sub-urban site PD, and are analyzed at a chemistry laboratory. The study on the  
147 O<sub>3</sub> chemical production in this paper is limited at XJH and PD by the intensive measurements of  
148 O<sub>3</sub> and its precursors (VOCs and NO<sub>x</sub>) from 2006 to 2015 at these two urban sites. The  
149 meteorological measurements including wind speed and direction, solar radiation and  
150 temperature are collected at BS site, which is the only climatology observatory in Shanghai. The  
151 meteorological measurements in BS are used for international exchange of meteorological data  
152 representing Shanghai, sponsored by the World Meteorological Organization (WMO). The  
153 geographical distribution of the 6 sites is indicated in Fig. 1.

154

155 **Figure 1.** (a) The distribution of topography height in Shanghai and its neighboring area. (b) The  
156 distribution of land-use category in Shanghai. The locations of the 6 sites (XJH, BS, PD, SS, JS, DT)  
157 are described by blue dots.

158

## 159 2.2 Instruments

160 O<sub>3</sub> is measured using an EC 9810 Ozone Analyzer, together with a UV photometer, which  
161 accurately and reliably measures O<sub>3</sub> concentration in ambient air. The oxides of nitrogen analyzer  
162 (EC9841B/ECOTECH) have a heated molybdenum NO<sub>2</sub> to NO converter. The resulting NO  
163 concentration is quantified using the chemiluminescence technique. This instrument has  
164 automated to set to be zero, and include an optional external valve manifold and external  
165 calibration sources. Quality control checks are performed every 3 days, including inspection of  
166 the shelter and instruments as well as zero, precision and span checks. Filter is replaced once  
167 every two weeks and calibration is made every month. The O<sub>3</sub> concentrations are recorded every  
168 1 min.

169 VOCs concentrations are sampled for 24 h every day with a 6 L silonite canister with a  
170 silonite coated valve (model 29-10622). The internal silonite coating improves long-term VOC  
171 storage. The instrument has a large volume to detect volatile chemicals down to low pptv range.  
172 Absorption is eliminated by using nupropackless valves and by eliminating teflon tape in the valve  
173 stem. These canisters are recognized to meet or exceed the technical specifications required for  
174 EP methods TO14-A and TO15. Gases samples are pre-processed using Model 7100 VOC  
175 preconcentrator. Samples are analyzed for VOCs using a gas chromatography system (Agilent  
176 GC6890) coupled with mass-selective detection (Agilent MSD5975 N) with length of 60 m,  
177 diameter of 0.32 mm, and film thickness of 1.0 μm. This measurement system can detect VOCs  
178 concentrations down to low pptv range.

179 These instruments to measure O<sub>3</sub>, NO<sub>x</sub> and VOCs concentrations are calibrated carefully.  
180 Detail information for the instruments and the procedures to perform data quality control are  
181 described by Geng et al. (2007), Ran et al. (2009), Tie et al. (2013) and Gao et al. (2017). These  
182 data have been widely used to investigate the diurnal, seasonal and inter-annual variations of O<sub>3</sub>  
183 in Shanghai (Geng et al., 2007; 2015; Tang et al., 2008; Ran et al., 2009; Gao et al., 2017) and its  
184 chemical mechanism (Geng et al., 2008a; 2008b; Tie et al., 2009a; 2013).

## 185 2.3 WRF-Chem model

186 The regional chemical/transport model (Weather Research and Forecasting Chemical model-



187 WRF-Chem) (Grell et al., 2005) is used to investigate the O<sub>3</sub> variations response to emission  
188 changes in Shanghai. The version of the model is improved mainly by Tie et al. (2007) and Li et al.  
189 (2010; 2011). The chemical mechanism chosen in WRF-Chem is the RADM2 (Regional Acid  
190 Deposition Model, version 2) gas-phase chemical mechanism (Stockwell et al., 1990), which  
191 includes 158 reactions among 36 species. The fast radiation transfer module (FTUV) is developed  
192 and used to calculate photolysis rates (Tie et al., 2003), considering the impacts of aerosols and  
193 clouds on the photochemistry (Li et al., 2011). The aerosol modules are developed by EPA CMAQ  
194 (version 4.6) (Binkowski and Roselle, 2003). The wet deposition of chemical species is calculated  
195 using the method in the CMAQ module and the dry deposition parameterization follows Wesely  
196 et al. (1989). The ISORROPIA version 1.7 is used to calculate the inorganic aerosols (Nenes et al.,  
197 1998). The secondary organic aerosol (SOA) is predicted using a non-traditional SOA module,  
198 including the volatility basis set (VBS) modeling approach and SOA contributions from glyoxal and  
199 methylglyoxal. The major physical processes employed in WRF are summarized as the Lin  
200 microphysics scheme (Lin et al., 1983), the Yonsei University (YSU) PBL scheme (Hong et al., 2006),  
201 the Noah Land surface model (Chen and Dudhia, 2001), and the long wave radiation  
202 parameterization (Dudhia, 1989).

203 The domain is set up to cover a region (centered at 32.5°N, 118°E) of 356 × 345 grids with  
204 a horizontal resolution of 6 km (Zhou et al., 2017). The initial and lateral boundary conditions of  
205 the meteorology are extracted from the NCEP FNL reanalysis data. The lateral meteorological  
206 boundary is updated every 6 h. The chemical lateral boundary conditions are constrained by the  
207 global chemical transport model (MOART—Model for Ozone and Related chemical Tracers) with  
208 aerosol formation modules (Tie et al., 2001; Emmonset al., 2010). Both the chemical and  
209 dynamical integration step is set as 60 s. The Multi-resolution Emission Inventory for China (MEIC)  
210 developed by Zhang et al. (2009) is used in WRF-Chem for the domain except Shanghai. The  
211 anthropogenic emissions (including CO, NO<sub>x</sub>, SO<sub>2</sub> and VOCs) for Shanghai are developed by Tie et  
212 al. (2013) based on the MIRAGE-shanghai field campaign. NO<sub>x</sub> and SO<sub>2</sub> emissions in YRD region  
213 are adjusted by Zhou et al. (2017) according to the performance evaluation of WRF-Chem  
214 prediction for about 195 cities during 2014–2015. The biogenic emissions are calculated online  
215 using the MEGAN (Model of Emissions of Gases and Aerosol from Nature) model developed by  
216 Guenther et al. (2006).

#### 217 **2.4 OZIPR model**

218 The ozone isopleths diagram for Shanghai is plotted by OZIPR (Ozone Isopleths Plotting Package  
219 Research) model (Gery and Crouse, 2002). The OZIPR model employs a trajectory-based air  
220 quality simulation model in conjunction with the Empirical Kinetics Modeling Approach (EKMA)  
221 to relate O<sub>3</sub> concentrations levels of organic and nitrogen oxide emissions. OZIPR simulates  
222 complex chemical and physical processes of the lower atmosphere through a trajectory model.  
223 The physical representation is a well-mixed column of air extending from the ground to the top of  
224 the mixed layer. Emissions from the surface are included as the air column passes over different  
225 emission sources, and air from above the column is mixed in as the inversion rises during the day.  
226 O<sub>3</sub> precursor concentrations and ambient information such as temperature, relative humidity and  
227 boundary layer height from measurements in Shanghai were specified for each single run.  
228 Therefore a series of simulations were performed to calculate peak O<sub>3</sub> concentration as a  
229 function of initial precursor concentrations (Tang et al., 2008; Geng et al., 2008b).



230

### 231 **3 Variability of O<sub>3</sub> and its precursors measured in Shanghai**

#### 232 **3.1 Variation of O<sub>3</sub> concentration**

233 Fig. 2a and b show the annual variation of O<sub>3</sub> concentration at downtown site XJH and sub-urban  
234 site PD respectively from 2006 to 2015. The O<sub>3</sub> concentrations increase notably during the past  
235 ten years with the increasing rate of 1.057 ppbv yr<sup>-1</sup> at XJH and 1.346 ppbv yr<sup>-1</sup> at PD respectively.  
236 It is consistent with the reported O<sub>3</sub> increasing trend ranging from 1-2 ppbv yr<sup>-1</sup> at background  
237 and urban sites in eastern China during 2001 to 2015 (Tang et al., 2009; Ma et al., 2016; Sun et al.,  
238 2016). In 2006, the mean O<sub>3</sub> concentrations at XJH and PD are 20 ppbv and 28 ppbv respectively.  
239 While in 2017, the mean O<sub>3</sub> concentrations at the two sites increase to 35 ppbv and 42 ppbv  
240 respectively, with 26% and 30% enhancement compared with that in 2006. The mean O<sub>3</sub>  
241 concentration at downtown site XJH during 2006 to 2015 is 32 ppbv, which is significantly lower  
242 than that at sub-urban site PD of 36 ppbv, suggesting the O<sub>3</sub> is depressed in downtown area.  
243 Geng et al. (2007) suggested that the O<sub>3</sub> production in the city of Shanghai was under  
244 VOC-limited regime, thus higher NO<sub>x</sub> in downtown resulted in lower O<sub>3</sub> concentration.  
245 Considering the inhomogeneous spatial distribution of the precursors of O<sub>3</sub> in Shanghai (Geng et  
246 al. 2008a), we extend the analysis on O<sub>3</sub> variations to a broader scope by using the O<sub>3</sub>  
247 measurements from 31 sites provided by Shanghai Environmental Monitoring Center, covering  
248 the entire Shanghai area. It is shown in Fig. 2c that the median of the O<sub>3</sub>-8h concentration also  
249 increases significantly from 2006 to 2015, with the increasing rate of 1.571 ppbv yr<sup>-1</sup>, indicating  
250 that the significant increasing trend of O<sub>3</sub> concentration not only occurs in the city of Shanghai,  
251 but also expanded to a larger area nearby Shanghai. Li et al. (2019) also reported a regional O<sub>3</sub>  
252 increasing phenomena in summer during 2013 to 2017 from Shanghai to Beijing in eastern China.

253 In order to analyze the individual contribution to the long-term O<sub>3</sub> trend, the variations of O<sub>3</sub>  
254 precursors, and meteorological parameters are measured and showed in the following sections.

255

256 **Figure 2.** The mean annual O<sub>3</sub> concentration (ppbv) from 2006 to 2015 at (a) downtown site XJH  
257 and (b) sub-urban site PD, both presenting the significant increasing trends with 1.057 ppbv yr<sup>-1</sup>  
258 at XJH and 1.346 ppbv yr<sup>-1</sup> at PD. The variation of the median 8-h O<sub>3</sub> concentration (ppbv) from  
259 2006 to 2015 averaged for 31 sites over Shanghai (c), also shows the increasing variability of  
260 1.571 ppbv yr<sup>-1</sup>.

261

#### 262 **3.2 Variations of the precursors (NO<sub>x</sub> and VOCs)**

263 It is well known that the tropospheric O<sub>3</sub> formation is throughout a complicated photochemical  
264 process, and is strongly related to the precursors of O<sub>3</sub> (VOCs and NO<sub>x</sub>). According to the previous  
265 studies (Geng et al., 2007; Ran et al., 2009), the chemical formation of O<sub>3</sub> in Shanghai is revealed  
266 to be under VOC-limited. Thus either enhancement of VOCs or reduction in NO<sub>x</sub> would both  
267 result in the growth of O<sub>3</sub> concentration. In order to better understanding the factors possibly  
268 driving the O<sub>3</sub> increasing trend depicted in Fig. 2, the variations of NO<sub>x</sub> and VOCs concentrations  
269 at XJH and PD in the same period are presented in Fig. 3. The NO<sub>x</sub> concentrations present  
270 significant decreasing trend from 2006 to 2015 at both XJH and PD sites, which is opposite to the  
271 increasing trend of O<sub>3</sub> variations in Fig. 2. At XJH, the decreasing rate of NO<sub>x</sub> is 2.15 ppbv yr<sup>-1</sup>,





272 which is more remarkable than that at PD site of  $1.86 \text{ ppbv yr}^{-1}$ . According to the studies by Lin et  
273 al (2017), the reduction of  $\text{NO}_x$  concentration in Shanghai was likely attributed to the  
274 implementation of stringent emission control strategy for transportation, including improvement  
275 of gas quality, popular usage of electricity cars, and limitation of heavy cars into the urban zones.  
276 These regulations significantly decrease the emissions of  $\text{NO}_x$  into the atmosphere, resulting in  
277 lower  $\text{NO}_x$  concentrations. Zheng et al. (2018) also reported the 30% reduction of  $\text{NO}_x$  emission in  
278 the past 5 years in YRD region. In comparison, the VOCs concentrations at XJH and PD decrease  
279 very slightly during 2006 to 2015. At XJH, the mean VOCs concentration during 2013 to 2015 is  
280 about 20 ppbv, which is some lower than that during 2009 to 2012 of 23 ppbv. At PD, the VOCs  
281 concentration shows strong inter-annual variations, ranging from 16 to 22 ppbv. Generally the  
282 VOCs concentration at the downtown site XJH is higher than that at the sub-urban site PD by 14%.  
283 It is consistent with the studies of Cai et al. (2010), suggesting that about 25% of VOCs is  
284 attributed to the vehicles in shanghai urban zones.

285

286 **Figure 3.** The mean annual concentrations (ppbv) of  $\text{NO}_x$  (dots) and VOCs (bars) from 2006 to  
287 2015 at (a) downtown site XJH and (b) sub-urban site PD respectively. The  $\text{NO}_x$  concentrations at  
288 XJH and PD both present obvious decreasing trends with  $-2.1 \text{ ppbv yr}^{-1}$  and  $-1.87 \text{ ppbv yr}^{-1}$ . While  
289 the VOCs concentrations at both sites present no clear inter-annual trends.

290

### 291 3.3 Meteorological impacts on $\text{O}_3$ photolysis, dispersion and transport

292 In addition to the precursors, meteorology such as solar radiation and wind speed and directions  
293 also plays the important roles in  $\text{O}_3$  concentration through the photochemical and physical  
294 processes. Fig. 4 shows the annual variation of wind speed and total solar radiation from 2006 to  
295 2015. The solar radiation presents weak annual variations ranging from  $140$  to  $150 \text{ Wm}^{-2}$ ,  
296 exhibiting a large variability but without a significant trend. As a result, the variation of solar  
297 radiation cannot explain the significant change of  $\text{O}_3$  concentration on the view of photolysis. The  
298 wind speed is usually regarded as the indicator for the dispersion capacity for air pollutants.  
299 Several studies reported that the wind speed in winter in eastern China presented decreasing  
300 variability during the past 40 years due to the decadal variation of winter monsoon affecting the  
301 haze occurrence (Wang et al., 2016; Zhao et al., 2016; Xu et al., 2017). While high  $\text{O}_3$  events  
302 usually occur in summer season for middle-latitude cities such as Shanghai (Wang et al., 2017).  
303 The mean summer wind speeds in Fig. 4a show slight decreasing from 2006 to 2015, while  
304 without significant trends. The wind speed fluctuates between  $3.3 \text{ ms}^{-1}$  to  $3.9 \text{ ms}^{-1}$  except the  
305 minimum value in 2014 ( $2.9 \text{ ms}^{-1}$ ) due to fewer typhoon in the period. Without 2014, the  
306 variability of summer wind speed is insignificant, with a trend of  $-0.02 \text{ m s}^{-1} \text{ yr}^{-1}$ , which could not  
307 be regarded as the dominant factor to interpret the increasing  $\text{O}_3$  trend. Local  $\text{O}_3$  concentration  
308 would be affected by transport of upstream plumes usually determined by wind direction. Geng  
309 et al. (2011) suggested that  $\text{O}_3$  concentration was higher in west wind compared with other wind  
310 sectors in Shanghai indicating the possible  $\text{O}_3$  transport from western area out of Shanghai. Fig. 5  
311 presents the annual wind rose at Baoshan site from 2006 to 2015, presenting the very similar  
312 pattern of wind direction in each year. The mean wind direction concentrates in the sector  
313 between  $60$ - $80$  degree, suggesting the dominant wind in Shanghai is easterly accounting for 50%.  
314 The east wind in Shanghai usually carries with the clean air mass from the sea to improve the





315 local air quality (Xu et al., 2015). The frequency of west wind changes little during 2006 and 2015  
316 ranging from 10-15%, suggesting that the regional transport is not a major factor driving the O<sub>3</sub>  
317 increasing. Based on the above analysis, it is speculated that the rapid O<sub>3</sub> increasing during  
318 2006–2015 in Shanghai is likely attributed to the reduction of NO<sub>x</sub> concentration as a result of the  
319 VOC-limited condition for O<sub>3</sub> production.

320

321 **Figure 4.** The annual variation of (a) summer wind speed (m s<sup>-1</sup>) and (b) total solar radiation (W  
322 m<sup>-2</sup>) from 2006 to 2015 in Shanghai. Both wind speed and the solar radiation present weak  
323 inter-annual variations but without significant trends.

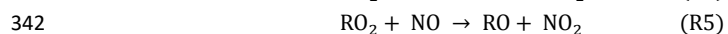
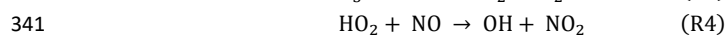
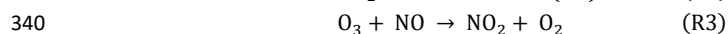
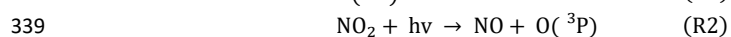
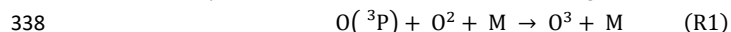
324

325 **Figure 5.** The wind rose in each year from 2006 to 2015 in Shanghai. The red line means the  
326 resultant vector suggesting the dominant wind direction.

327

### 328 3.4 Different O<sub>3</sub> variability in nighttime and daytime

329 To further qualify the changes of O<sub>3</sub> precursors, especially NO<sub>x</sub> on the measured O<sub>3</sub> variability,  
330 intensive model studies are applied. At first, a brief O<sub>3</sub> daytime and nighttime chemistry is  
331 described. As we know, O<sub>3</sub> in the Earth's atmosphere is ultimately formed from the combination  
332 reaction of atomic oxygen (O<sup>3</sup>P) and molecular oxygen (O<sub>2</sub>) (R1). In the troposphere with little UV  
333 radiation, photolysis of NO<sub>2</sub> at wavelengths ≤424 nm (R2) is the primary source of O<sup>3</sup>P atoms  
334 and prompts O<sub>3</sub> production. Once formed, O<sub>3</sub> readily lost with reaction with NO to converts back  
335 to NO<sub>2</sub> (R3). The (R1-R3) reactions result in a null cycle when no other chemical species are  
336 involved. However, in reality, the troposphere contains alternative oxidants (i.e., HO<sub>2</sub> and RO<sub>2</sub>)  
337 that efficiently convert NO to NO<sub>2</sub> (R4 and R5), resulting in the accumulation of O<sub>3</sub>.



343 The O<sub>3</sub> chemical mechanism in daytime includes both production and loss processes. In  
344 contrast, in nighttime, the photochemical production ceases, and there mainly exists loss process  
345 for O<sub>3</sub>. Fig. 6 shows the O<sub>3</sub> variations in daytime and nighttime respectively from 2006 to 2015 at  
346 XJH and PD sites. Both daytime and nighttime O<sub>3</sub> concentrations present significant increasing  
347 trend at two sites, which is consistent with the results in Fig. 2. It is worthy to note that O<sub>3</sub>  
348 concentration in nighttime increases more rapidly than that in daytime. For example, at XJH the  
349 nighttime O<sub>3</sub> concentration increases at the rate of 1.47 ppbv yr<sup>-1</sup> from 2006 to 2015, higher than  
350 that in daytime of 0.85 ppbv yr<sup>-1</sup>. At PD, the increasing rate of O<sub>3</sub> concentration is 1.22 ppbv yr<sup>-1</sup>  
351 in nighttime, also higher than that in daytime of 0.91 ppbv yr<sup>-1</sup>. These results suggest that the  
352 reduction of NO<sub>x</sub> concentration from 2006 to 2015 has different effects on daytime and nighttime  
353 O<sub>3</sub> variations. The O<sub>3</sub> concentration in nighttime is more sensitive to NO<sub>x</sub> reduction, resulting in  
354 less O<sub>3</sub> lost compared with that in daytime. The results in Fig. 6 also show that the increasing rate  
355 of nighttime O<sub>3</sub> in downtown site XJH is higher than that at sub-urban site PD due to the more  
356 reduction of NO<sub>x</sub> concentration in downtown area.

357



358

359 **Figure 6.** The annual variations of daytime and nighttime O<sub>3</sub> concentration (ppbv) from 2006 to  
360 2015 at (a) downtown site XJH and (b) sub-urban site PD.

361

#### 362 **4 WRF-Chem study on the O<sub>3</sub> variation response to emission change**

##### 363 **4.1 Design of the model experiments scheme**

364 To better understand the role of NO<sub>x</sub> emission reduction in O<sub>3</sub> variation, the WRF-Chem model is  
365 utilized to calculate the changes of O<sub>3</sub> concentrations. Lin et al. (2017) suggested that the NO<sub>x</sub>  
366 emission was reduced in Shanghai in recent years resulted from the implementation of the  
367 Shanghai Clean Air Action Plan. The NO<sub>x</sub> emission in 2015 is estimated at  $33.4 \times 10^4$  ton in  
368 Shanghai, reduced significantly by 30% compared with that in 2009 of  $44.9 \times 10^4$  ton. Thus it  
369 provided the good opportunity to examine the O<sub>3</sub> variation response to the reduction of NO<sub>x</sub>  
370 emission in Shanghai. The NO<sub>x</sub> emissions in 2009 and 2015 are put into WRF-Chem model  
371 respectively to calculate the O<sub>3</sub> concentration. The other emissions (including gas and particulate  
372 matter) and meteorology used in WRF-Chem are set same. As a result, the difference of O<sub>3</sub>  
373 concentrations calculated by WRF-Chem is solely attributed to the change of NO<sub>x</sub> emission  
374 between 2009 and 2015, which is furthermore compared with the measurements.

375 The MIRAGE-shanghai field campaign was conducted in September of 2009 to explore the  
376 O<sub>3</sub> chemical formation and transformation in Shanghai (Tie et al., 2013). The mean temperature,  
377 mean wind speed and total precipitation in this month is 25 °C, 2.85 m s<sup>-1</sup> and 89.5 mm  
378 respectively, which is very close to the climatological conditions during the past ten years from  
379 2006 to 2015, with 24.7 °C for mean temperature, 2.81 m s<sup>-1</sup> for mean wind speed, and 126 mm  
380 for total precipitation respectively. In addition, Shanghai is located at the typical sub-tropical area.  
381 The meteorology in September is characterized as the low cloud cover and rain occurrence, the  
382 slight wind speed and humidity, as well as the moderate solar radiation intensity. As suggested by  
383 Tie et al. (2013), the chemical age of O<sub>3</sub> plume in Shanghai urban area in September of 2009 was  
384 very young, indicating that the O<sub>3</sub> production was more dependent on the local emissions under  
385 such kind of meteorology, hence providing more insights into the O<sub>3</sub> chemical mechanism  
386 response to the local emission changes. We chose the meteorology in September of 2009 as the  
387 atmospheric background for the following sensitive experiments by WRF-Chem.

388 Tie et al. (2009a; 2013) highlighted that the WRF-Chem model was capable of studying the  
389 chemical and physical processes of O<sub>3</sub> in September of 2009 during the MIRAGE-Shanghai  
390 campaign. The calculated O<sub>3</sub>, NO<sub>x</sub>, VOCs and aerosols by WRF-Chem in clean and polluted  
391 episodes are fairly in agreement with the measurements except HONO, suggesting that the  
392 emission inventory in 2009 used in the model is reasonable for the Shanghai region. Moreover  
393 the VOCs emission in Shanghai is greatly improved according to the measurements from the  
394 MIRAGE-shanghai field campaign by Tie et al. (2013). Such emission from Tie et al. (2013)  
395 representing 2009 scenario is used in this study to conduct the control experiment (T1) as the  
396 baseline to simulate the O<sub>3</sub> and NO<sub>x</sub> concentrations in September of 2009. The T1 experiment is  
397 composed of 30 model runs for each day in September of 2009. Each model run is initiated at the  
398 20:00 (LST) and performed for 52 h integrations. The first 28 h integration is regarded as model  
399 spin-up periods, the results from the later 24 h integration is captured hourly and averaged for  
400 mean daily concentration of O<sub>3</sub> and NO<sub>x</sub>. The aim of the T1 experiment is to further evaluate the



401 reliability of the emission inventory in 2009 used in WRF-Chem by fully comparing the calculated  
402 O<sub>3</sub> and NO<sub>x</sub> concentrations with in-situ measurements of 6 sites over Shanghai.

#### 403 **4.2 The NO<sub>x</sub> emission in 2009 used for base experiment**

404 Fig. 7 showed the distribution of NO<sub>x</sub> emission of 2009 scenario (Tie et al., 2013) in Shanghai  
405 used in WRF-Chem model. The NO<sub>x</sub> emission is mostly distributed in the urban zones, suggesting  
406 that transportation is the important source. The NO<sub>x</sub> is largely exported in downtown and two  
407 neighboring sub-urban zones in the east and north respectively. The maximum NO<sub>x</sub> emission is  
408 estimated at 16 kg hr<sup>-1</sup> km<sup>-2</sup> at downtown, compared with 2-6 kg hr<sup>-1</sup> km<sup>-2</sup> in the sub-urban area.  
409 In addition, there is a small town located in the south of Shanghai with the similar intensity of  
410 NO<sub>x</sub> emission as the sub-urban zones. The total NO<sub>x</sub> emission of 2009 scenario in Shanghai (Fig. 7)  
411 is estimated at 41.4 × 10<sup>4</sup> ton in the model, which is close to the 47.8 × 10<sup>4</sup> ton suggested by Lin  
412 et al. (2017) according to the Shanghai Environmental Year Book.

413

414 **Figure 7.** The distribution of NO<sub>x</sub> emission (kg km<sup>-2</sup> h<sup>-1</sup>) in 2009 in Shanghai.

415

#### 416 **4.3 Performance evaluation on the base experiment**

417 The mean monthly O<sub>3</sub> concentration in September 2009 is calculated by WRF-Chem and  
418 compared with measurements over 6 sites in Shanghai. It is shown in Fig. 8 that both model  
419 simulations and in-situ measurements highlight the lower O<sub>3</sub> concentration in urban zones than  
420 that in suburb. The simulated O<sub>3</sub> concentration in downtown is 22-24 ppbv, significantly lower  
421 than that at sub-urban (30-35 ppbv) and rural area (40 ppbv), which is consistent with the  
422 measurements. The measured O<sub>3</sub> concentration at downtown site XJH is 22 ppbv, lower than that  
423 at sub-urban site PD and remote site DT by 12 ppbv and 26 ppbv respectively. Geng et al. (2007)  
424 suggested that under VOC-limited regime, the lower O<sub>3</sub> concentration in downtown was resulted  
425 from the higher NO<sub>x</sub> emission, which depressed the O<sub>3</sub> production process. Under high NO<sub>x</sub>  
426 conditions, the OH radicals are lost by the reaction of NO<sub>2</sub> + OH → HNO<sub>3</sub> (Sillman, 1995). As  
427 a result, higher NO<sub>x</sub> concentration in urban area leads to lower OH concentration, which results  
428 in smaller O<sub>3</sub> production. Tang et al. (2008) also suggested that the O<sub>3</sub> concentration in Shanghai  
429 downtown was higher at weekends than that on weekdays due to the reduced NO<sub>x</sub> concentration.  
430 However the discrepancy is also evident between model results and measurements. For example,  
431 the modeled O<sub>3</sub> concentrations at XJH and PD are about 2-3 ppbv higher than the measurements,  
432 perhaps due to the uncertainty of NO<sub>x</sub> and VOCs emission in urban area suggested by Tie et al.  
433 (2009a). In addition, the calculated O<sub>3</sub> concentrations in the remote site DT and chemical site JS  
434 are lower than measurements by 8 and 5 ppbv respectively. The former is resulted from the  
435 overestimation of the wind speed by WRF-Chem model leading to excessive O<sub>3</sub> transport for  
436 underestimation (Zhou et al., 2017). While the latter is mainly due to the prominent  
437 underestimation of the VOCs emission in the chemical zones suggested by Tie et al. (2009a).

438

439 **Figure 8.** The calculated distribution of O<sub>3</sub> concentration by WRF-Chem (shade) in September of  
440 2009 compared with measurements (circles) of 6 sites over Shanghai.

441

442 Fig. 9a and b show the daily variations of O<sub>3</sub> and NO<sub>x</sub> concentrations compared between



443 WRF-Chem simulations and the in-situ measurements over 5 sites. The statistical analysis of  
444 model performance for O<sub>3</sub> and NO<sub>x</sub> is listed in Table 1 and Table 2 respectively. The calculated  
445 magnitude and daily variation of O<sub>3</sub> concentrations agree well with the measurements,  
446 suggesting that both meteorology and photochemistry are well reproduced by WRF-Chem model.  
447 For example, the Root Mean Square Error (RMSE) calculated between modeled and measured O<sub>3</sub>  
448 concentration are 7.4, 10.5, 12, 8.6, 9.2 ppbv for XJH, JS, DT, PD and BS respectively, and the  
449 difference between the simulation results and in-situ measurement is below 10%, which are very  
450 satisfactory compare with the similar works by Geng et al (2007) and Tie et al. (2013). The  
451 correlated coefficients (R) for the mean daily O<sub>3</sub> concentration range from 0.6 to 0.8 above 99%  
452 confidence over 5 sites, indicating good consistency of day by day variations between the model  
453 results and measurements. Comparably the O<sub>3</sub> concentration is best simulated by WRF-Chem at  
454 the downtown site XJH and sub-urban site PD with the lower RMSE and better R. However the  
455 discrepancy of daily O<sub>3</sub> concentration between the model and measurements is also evident. For  
456 example, a rapid change of O<sub>3</sub> concentration from 16 to 19 in September was observed over all  
457 sites, indicating it's a regional event instead of a local phenomenon. The O<sub>3</sub> concentration firstly  
458 increases significantly during 16-19 (episode-1), then sharply decreased during the later 4 days  
459 (episode-2). The similar rapid O<sub>3</sub> change in Shanghai was also reported by Tie et al. (2009a), and  
460 their explanation is that this episode was mainly related to the intensity of the sub-tropical  
461 high-pressure system on Pacific Ocean in summer. The model captures the O<sub>3</sub> variations and  
462 magnitudes during the both risen and fallen episodes very well at downtown site XJH, but  
463 substantially underestimates the increasing variability of O<sub>3</sub> concentration during episode-1 at  
464 sub-urban and rural sites by 10-15 ppbv. Geng et al. (2008a) suggested the "chemical transport of  
465 O<sub>3</sub>" from Shanghai downtown area to the distance of 18-36 km far away, which increased the O<sub>3</sub>  
466 concentration at sub-urban or rural sites. This "chemical transport of O<sub>3</sub>" is difficult to be  
467 reflected by WRF-Chem model due to the current inventory is too coarse to accurately reflect the  
468 detailed distribution and variation of NO<sub>x</sub> emission, e.g. the NO<sub>x</sub> emission from mobile source in  
469 the city. In addition, the underestimation of the O<sub>3</sub> concentration at suburb of Shanghai in  
470 summer is possibly attributed to the model bias of sea breeze simulations. Under the condition of  
471 weak sub-tropical pressure, the sea breeze develops at noontime to yield a cycling wind pattern  
472 in Shanghai, leading to the rapid accumulation of high O<sub>3</sub> concentration. The WRF-Chem usually  
473 underestimates the sea surface temperature, which tends to accelerate the sea breeze  
474 development and weak the O<sub>3</sub> trapping in the city (Tie et al., 2009a). The calculated daily NO<sub>x</sub>  
475 concentration by WRF-Chem compared with measurements are shown in Fig. 9b. Both the  
476 modeled and measured NO<sub>x</sub> concentrations at the remote site DT are very low, with the average  
477 of 1.4 and 2.9 ppbv respectively due to seldom anthropogenic emissions there. The calculated  
478 NO<sub>x</sub> concentration at XJH and PD are generally well consistent with the measurements with the  
479 excellent R of 0.8 and 0.82 and small RMSE of 6.9 and 7.5 ppbv respectively. However the NO<sub>x</sub>  
480 concentration is underestimated by WRF-Chem at sub-urban site BS in the steel zone. The  
481 calculated NO<sub>x</sub> concentration at BS is 16.1 ppbv, which is lower than the measurements by 5 ppbv.  
482 The difference of NO<sub>x</sub> concentrations between the model and observations is generally above  
483 10%, suggesting the performance of NO<sub>x</sub> simulation is somewhat lower than that of O<sub>3</sub>. It was  
484 also reported by Tie et al. (2007; 2009b; 2013), during the evaluation of the NO<sub>x</sub> calculations by  
485 WRF-Chem in MIRAGE-Shanghai and MIRAGE-mex campaign studies. The lifetime of NO<sub>x</sub> at the  
486 surface is about 1-2 days, shorter than O<sub>3</sub>. Thus the NO<sub>x</sub> concentration is determined by the



487 detailed emissions and dynamical factors, which need to develop the advanced inventory with  
488 higher resolution to reproduce both the spatial distributions and temporal variations of NO<sub>x</sub>  
489 emission.

490

491 **Figure 9.** The calculated mean daily concentrations (ppbv) of (a) O<sub>3</sub> and (b) NO<sub>x</sub> at 5 sites in  
492 September of 2009 by WRF-Chem (red circles) and compared with measurements (blue circles).

493

#### 494 4.4 Sensitive study on the O<sub>3</sub> variability response to the emission change

495 The T1 experiment shows the excellent performance for O<sub>3</sub> and NO<sub>x</sub> simulations, including the  
496 spatial distribution pattern, and the day by day variation and magnitude. It is indicated that the  
497 emission in 2009 scenario used in WRF-Chem is reasonable, and the model is efficient for  
498 conducting the sensitive studies on O<sub>3</sub> variation response to the emission change. In order to  
499 better understand the measured long-term trend of O<sub>3</sub> concentration during the past ten years in  
500 Shanghai and its relationship to the emission reduction, several sensitive studies are conducted in  
501 this study (Table 3). The control study of T1 is conducted based on the NO<sub>x</sub> emission in 2009  
502 scenario in Shanghai. According to the study of Lin et al. (2017), the NO<sub>x</sub> emission in 2015 in  
503 Shanghai is reduced by 30% compared with that in 2009. Thus we conduct the sensitive  
504 experiment T2 by WRF-Chem, cutting the NO<sub>x</sub> emission by 30% compared with T1, whereas  
505 keeping the other emissions and meteorology same as T1. As a result, the calculated O<sub>3</sub>  
506 difference between T1 and T2 is likely attributed to the NO<sub>x</sub> emission reduction between 2015  
507 and 2009.

508 Fig. 10a shows the distribution of the difference of O<sub>3</sub> concentration simulated by T1 and T2  
509 (T2-T1). The reduction of NO<sub>x</sub> emission has the obvious effect on the magnitude and distribution  
510 of O<sub>3</sub> concentration. The O<sub>3</sub> concentration increases notably in urban area corresponding to the  
511 higher NO<sub>x</sub> emissions in Fig. 7, ranging from 2-7 ppbv. The enhancement of O<sub>3</sub> concentration is  
512 most significant in downtown and neighboring sub-urban zones, as well as the southern town,  
513 generally more than 4 ppbv. For example, the maximum increase in O<sub>3</sub> concentration is 6.4 ppbv  
514 occurred at downtown site XJH, followed by 4-5 ppbv at sub-urban site PD. The increasing rates  
515 of O<sub>3</sub> trend at XJH and PD are estimated at 1.06 ppbv yr<sup>-1</sup> and 0.96 ppbv yr<sup>-1</sup> from 2009 to 2015  
516 by WRF-Chem, which is consistent to the observed O<sub>3</sub> growth variability (Fig. 2) of 1-1.3 ppbv yr<sup>-1</sup>.  
517 The response of O<sub>3</sub> concentration to the NO<sub>x</sub> reduction is not evident in the rural area including  
518 the eastern part of Shanghai and the island with low NO<sub>x</sub> emissions. The comparison of T1 and T2  
519 further illustrates the speculation that the significant increasing trend of O<sub>3</sub> concentration during  
520 the past ten years in Shanghai is mostly attributed to the reduction of NO<sub>x</sub> emission as a result of  
521 the implementation of Shanghai Clean Air Action Plan.

522 The O<sub>3</sub> chemical formation is strongly related to NO<sub>x</sub> and VOCs concentrations. As discussed  
523 by Geng et al. (2008a) the O<sub>3</sub> chemical formation is clearly under VOC-limited regime in Shanghai  
524 and its neighboring area. Under the high NO<sub>x</sub> condition, NO tends to react with O<sub>3</sub> instead of NO<sub>2</sub>,  
525 flowing by NO<sub>2</sub> + OH → HNO<sub>3</sub>, causing the decrease of the reactivity and ensuing O<sub>3</sub>  
526 concentrations. Thus reduced NO<sub>x</sub> emission would result in increase in O<sub>3</sub> concentration, which  
527 has been discussed in Fig. 10a.

528 Despite of minor change of VOCs in the last ten years, it is worth to investigate the effect of  
529 the VOCs changes on O<sub>3</sub> concentrations in Shanghai. For this purpose, we conduct a sensitive



530 study (T3), with 50% increase of VOCs emission compared with T1, but keeping  $\text{NO}_x$  and other  
531 emissions as well as the meteorology same as T1. For RADM2 gas mechanism used in WRF-Chem,  
532 the VOCs are surrogated into 14 species, such as alkane, alkene, aromatic, formaldehyde, etc. All  
533 the species of VOCs are increased by 50% at every model grid over Shanghai and at every hour.  
534 The difference of  $\text{O}_3$  concentration between T3 and T1 (T3-T1) is shown in Fig. 10b. As we  
535 expected, the  $\text{O}_3$  concentration in Shanghai is sensitive to the enhancement of VOCs emission,  
536 increased by 3-4 ppbv in urban area due to more NO is converted to  $\text{NO}_2$  by reaction with  $\text{RO}_2$   
537 and  $\text{HO}_2$ . Furthermore, the abundant  $\text{O}_3$  plumes produced in the urban zones significantly  
538 transport to the downwind areas about 100-200 km away, resulting in elevated  $\text{O}_3$  concentration  
539 in the western Shanghai by about 2 ppbv. According to Tie et al. (2013), the  $\text{O}_3$  plume released in  
540 Shanghai urban area can be transported to downwind of the city by about 100-150 km away in  
541 the MIRAGE-shanghai field campaign. The model studies of T1, T2 and T3 highlight that under the  
542 emission of 2009 scenario, the  $\text{O}_3$  chemical production is clearly under VOC-limit regime, either  
543 decreasing  $\text{NO}_x$  concentration or increasing VOCs concentration would result in the  $\text{O}_3$   
544 enhancement. The analysis on in-situ measurements and model experiments jointly suggests that  
545 the significant  $\text{O}_3$  increasing trend during the past ten years in Shanghai is mainly attributed to  
546 the large reduction of  $\text{NO}_x$  emission.

547

548 **Figure 10.** The difference of  $\text{O}_3$  concentration (ppbv) between (a) T2 and T1 (T2-T1), (b) T3 and  
549 T1 (T3-T1) respectively conducted by WRF-Chem model. The difference between T2 and T1 lies in  
550 the  $\text{NO}_x$  emissions set in T2 (2015 scenario) is 30% lower than that in T1 (2009 scenario), which is  
551 estimated by Lin et al. (2017) according to the Shanghai Environment Yearbook. The difference  
552 between T3 and T1 is dependent on that the VOCs emission in T3 is 50% higher than that in T1.

553

#### 554 4.5 The variation of $\text{O}_3$ production regime response to emission change

555 The  $\text{O}_3$  chemical mechanism in Shanghai was explored by several studies based on the in-situ  
556 measurements around 2008 and 2009. Geng et al. (2008a; 2008b), Ran et al. (2009) and Tie et al.  
557 (2009a) all revealed that the  $\text{O}_3$  production around 2008 and 2009 in Shanghai was clearly under  
558 VOC-limit regime which was further illustrated by the above model studies. As indicated in Fig. 3,  
559 the significant decrease of  $\text{NO}_x$  concentration is observed from 2009 to 2015 in Shanghai, while  
560 the VOCs concentration changed little during the same period. As we know, the  $\text{O}_3$  chemical  
561 formation is strongly related to  $\text{NO}_x$  and VOCs concentrations with nonlinearity. Thus the  
562 different variability of  $\text{NO}_x$  and VOCs concentration from 2009 to 2015 inevitably has the large  
563 effect on the  $\text{O}_3$  production regime, which need to be investigated deeply.

564 The complex relationship among  $\text{NO}_x$ , VOCs and  $\text{O}_3$  concentrations is usually depicted by  $\text{O}_3$   
565 isopleths diagram. The  $\text{O}_3$  isopleths plot (Fig. 11) in Shanghai used in this study is constructed by  
566 the OZIPR model based on the in-situ measurements of  $\text{O}_3$ ,  $\text{NO}_x$ , VOCs and meteorology. Under  
567 high VOCs and low  $\text{NO}_x$  condition (low  $\text{NO}_x/\text{VOCs}$  ratio), the  $\text{O}_3$  production is not sensitive to  
568 VOCs, while positively correlated to  $\text{NO}_x$  concentration, which is viewed as  $\text{NO}_x$ -limited regime. By  
569 contrast, under low VOCs and high  $\text{NO}_x$  condition (high  $\text{NO}_x/\text{VOCs}$  ratio), the  $\text{O}_3$  production tends  
570 to increase with the VOCs growth or  $\text{NO}_x$  reduction, which is regarded as VOC-limited regime. The  
571  $\text{NO}_x$ -limited and VOC-limited regime is divided by a ridge line (the dot-dash line in Fig. 11) in the  
572  $\text{O}_3$  isopleths plot. The  $\text{O}_3$  production is not sensitive to neither  $\text{NO}_x$  concentration nor VOCs



573 concentration when near the ridge line, which is regarded as the transition regime.

574 The O<sub>3</sub> chemical production regime at XJH and PD in 2009 and 2015 is positioned  
575 respectively in Fig. 11. In 2009 the O<sub>3</sub> production at both XJH and PD sites (marked as red and  
576 blue hollow circle respectively) are clearly under VOC-limited regime. Thus decrease in NO<sub>x</sub>  
577 concentration leads to the O<sub>3</sub> enhancement, which is highlighted by the previous in-situ  
578 measurements and model experiments. Since then the O<sub>3</sub> production regime tends to move  
579 toward the dot-dash line due to the significant reduction of NO<sub>x</sub> concentration accompanied with  
580 the relative less change of VOCs at the two sites. In 2015 the O<sub>3</sub> production at XJH (marked as red  
581 solid circle) is still under VOC-limited regime, but for PD (marked as blue solid circle), it is close to  
582 the dot-dash line, approaching the transition regime between VOC-limited to NO<sub>x</sub>-limited. This  
583 result suggests that if the NO<sub>x</sub> emission keeps reduction after 2015 assuming the VOCs  
584 concentration keeps constant, the O<sub>3</sub> concentration will continue to increase at XJH, while at PD  
585 the O<sub>3</sub> concentration is supposed to be insensitive to the NO<sub>x</sub> change. According to the O<sub>3</sub>  
586 chemical regime depicted in Fig. 11, if the NO<sub>x</sub> concentration decreases by 5 ppbv after 2015, the  
587 peak O<sub>3</sub> concentration at XJH will further increase by 3 ppbv, whereas at PD it seems to change  
588 very slightly. To better understand this further change, more sensitive studies of WRF-Chem are  
589 conducted in the following sections.

590

591 **Figure 11.** The O<sub>3</sub> chemical production at downtown site XJH and sub-urban site PD in 2009 and  
592 2015 depicted by O<sub>3</sub> isopleths diagram. The hollow and solid red circles denote O<sub>3</sub> production  
593 regime at XJH in 2005 and 2019 respectively. The hollow and solid blue circles denote O<sub>3</sub>  
594 production regime at PD in 2005 and 2019 respectively

595

## 596 5 The future O<sub>3</sub> evaluation

### 597 5.1 The O<sub>3</sub> level in 2020

598 According to the Shanghai Clean Air Action Plan, the NO<sub>x</sub> emission in Shanghai will be further  
599 reduced by 20% in 2020 compared with that in 2015. According to the above analysis based on  
600 the O<sub>3</sub> isopleths plot (Fig. 11), the O<sub>3</sub> concentrations in downtown and sub-urban seem to have  
601 distinct different responses to further NO<sub>x</sub> reduction after 2015. In order to better understand  
602 the future O<sub>3</sub> variation, the sensitive experiment T4 is conducted by WRF-Chem with 20%  
603 reduction of NO<sub>x</sub> emission compared with T2. T2 and T4 represent the NO<sub>x</sub> emission in 2015 and  
604 2020 respectively. The other emissions and meteorology are set to be same as T1. The difference  
605 of O<sub>3</sub> concentration between T2 and T4 (T4-T2) is presented in Fig. 12a. The O<sub>3</sub> concentration  
606 keeps increasing in downtown area such as XJH site, ranging from 2-4 ppbv. However, for the  
607 sub-urban zones such as the PD site, the O<sub>3</sub> concentration changes very little response to the  
608 further NO<sub>x</sub> reduction, ranging from 0-1 ppbv. As discussed in Fig. 11, in 2015 the O<sub>3</sub> production  
609 at PD is possibly under the transition regime from VOC-limited to NO<sub>x</sub>-limited near the ridge line.  
610 As a result, the O<sub>3</sub> concentration is not sensitive to the variation of NO<sub>x</sub> concentration. However  
611 the O<sub>3</sub> concentration in the suburb zones generally decreases by 1ppbv, indicating that with the  
612 further NO<sub>x</sub> reduction after 2015 the O<sub>3</sub> chemical production transfers from VOCs-limited to  
613 NO<sub>x</sub>-limited regime in the rural of Shanghai.

614 It is suggested in Fig.11 that the O<sub>3</sub> production at downtown site XJH in 2015 is still under  
615 VOC-limited regime despite of the significant NO<sub>x</sub> reduction. The O<sub>3</sub> concentration would be also





616 sensitive to the variation of VOCs concentration. Thus the sensitive experiment T5 is conducted  
617 by WRF-Chem model with 50% enhancement of VOCs emission compared with T2 (representing  
618 the emission in 2015 scenario). It is presented in Fig. 12b that the O<sub>3</sub> concentration increases by  
619 2-3 ppbv in downtown area due to the enhancement of VOCs, suggesting that the O<sub>3</sub> production  
620 at downtown in 2015 is still under VOC-limited regime, which is consistent with the results in Fig.  
621 11. Moreover the O<sub>3</sub> plumes produced in urban area transport to the downwind area to  
622 accumulate the high O<sub>3</sub> concentration in the western area to Shanghai by 2 ppbv. While at  
623 sub-urban site PD, the O<sub>3</sub> concentration changes less than 1 ppbv response to the increase in  
624 VOCs emission, which is similar as the very weak O<sub>3</sub> variations relative to the NO<sub>x</sub> reduction in Fig.  
625 12a. Overall, the models studies of T4 and T5 jointly suggest that the O<sub>3</sub> concentration at  
626 sub-urban site PD in 2015 is not sensitive to either NO<sub>x</sub> or VOCs variations due to the O<sub>3</sub>  
627 production is under the transition regime depicted in the O<sub>3</sub> isopleths plot.

628  
629 **Figure 12.** The difference of O<sub>3</sub> concentration (ppbv) between (a) T4 and T2 (T4-T2), (b) T5 and  
630 T2 (T5-T2) respectively conducted by WRF-Chem model. The difference between T4 and T2 is  
631 that the NO<sub>x</sub> emissions set in T4 (2020 scenario) is 20% lower than that in T2 (2015 scenario),  
632 which is estimated according to the Shanghai Clean Air Action Plan. The difference between T5  
633 and T2 lies in that the VOCs emission in T5 is 50% higher than that in T2.  
634

## 635 5.2 The O<sub>3</sub> chemical production after 2020

636 The above study shows that the O<sub>3</sub> production at sub-urban site PD in 2020 will likely transfer  
637 from VOCs-limited regime to NO<sub>x</sub>-limited regime without consideration of possible VOCs changes.  
638 For the purpose of the O<sub>3</sub> pollution control strategy, it is worth to estimate the O<sub>3</sub> level response  
639 to emission change after 2020 in Shanghai. It is also essential to access how many NO<sub>x</sub> emission  
640 need to be cut after 2020 will cease the O<sub>3</sub> enhancement in downtown area. Thus the sensitive  
641 experiment T6 is conducted by further 20% reduction of NO<sub>x</sub> emission from 2020 scenario (T4).  
642 The difference of O<sub>3</sub> concentration between T6 and T4 (T6-T4) is shown in Fig. 13a. It is clear that  
643 the O<sub>3</sub> concentration at downtown keeps nearly constant regardless of the further reduction of  
644 NO<sub>x</sub> emission after 2020. That is to say the increasing trend of O<sub>3</sub> in downtown with the NO<sub>x</sub>  
645 reduction ceases after 2020, indicating that the O<sub>3</sub> production likely approaches the transition  
646 regime. In addition, the O<sub>3</sub> concentration decreases significantly out of the downtown area,  
647 ranging from 2-3 ppbv in sub-urban zones, and more than 4 ppbv in suburb, indicating that the  
648 O<sub>3</sub> production in Shanghai transfers to NO<sub>x</sub>-limited regime after 2020 except the downtown area  
649 where the O<sub>3</sub> production is likely near the transition zone. On the other hand, if the NO<sub>x</sub> emission  
650 is kept constant after 2020 as T4, while the VOCs emission is increased by 50% conducted in T7  
651 experiment, the O<sub>3</sub> concentration (Fig. 13b) changes little in both urban and suburb area in  
652 Shanghai which is different from the previous model study of T5 the T3 when O<sub>3</sub> production is  
653 under VOC-limited condition. It is suggested that the O<sub>3</sub> concentration after 2020 is not sensitive  
654 to the variation of VOCs concentration because the continuous reduction of NO<sub>x</sub> emission keeps  
655 in promoting the O<sub>3</sub> production to transfer into NO<sub>x</sub>-limited regime. Thus further reduction of  
656 NO<sub>x</sub> tends to decrease the O<sub>3</sub> concentration in Shanghai.

657  
658 **Figure 13.** The difference of O<sub>3</sub> concentration (ppbv) between (a) T6 and T4 (T6-T4), (b) T7 and



659 T4 (T7-T4) respectively conducted by WRF-Chem model. The NO<sub>x</sub> emissions set in T6 is 20% lower  
660 than that in T4 (2020 scenario). The VOCs emission in T7 is 50% higher than that in T4.

661

## 662 Conclusions

663 O<sub>3</sub> pollution is a serious issue in China. Better understanding the elevated O<sub>3</sub> and its response to  
664 emission change is important for Chinese megacities. In this study, we analyze the increasing  
665 trend of O<sub>3</sub> concentration by long-term measurements of O<sub>3</sub> and its precursors as well as  
666 meteorology in Shanghai combined with the WRF-Chem model. The O<sub>3</sub> production regime  
667 response to the emission change in Shanghai during the past ten years is also explored by O<sub>3</sub>  
668 isopleths plot. In addition, the future O<sub>3</sub> variation and its chemical production in Shanghai are  
669 evaluated by WRF-Chem model. The main conclusions are summarized as follows:

670 (1) The O<sub>3</sub> concentration measured in Shanghai increased significantly from 2006 to 2015  
671 with the rate of 1.057 ppbv yr<sup>-1</sup> at downtown site XJH and 1.346 ppbv yr<sup>-1</sup> at sub-urban site PD  
672 respectively. The observed increasing trend of O<sub>3</sub> is not limited in the urban zones but expanded  
673 to the larger scale covering the total Shanghai city. The NO<sub>x</sub> and VOCs concentrations presented  
674 different variability from O<sub>3</sub> during the same period, in which NO<sub>x</sub> concentration decreases  
675 significantly at both XJH and PD sites, whereas the VOCs changes very little without evident  
676 trend.

677 (2) Because there are minor trends of measured O<sub>3</sub> photolysis, local dispersion and regional  
678 transport resulted from meteorology, it is speculated that the significant O<sub>3</sub> increasing trend  
679 during 2006 to 2015 in Shanghai is likely attributed to the reduction of NO<sub>x</sub> concentration as a  
680 result of the strong VOCs-limited regime for O<sub>3</sub> production. The nighttime O<sub>3</sub> is more sensitive to  
681 NO<sub>x</sub> reduction than that in daytime, because of more O<sub>3</sub> is depressed by NO<sub>x</sub> in nighttime. As a  
682 result, the observed nighttime O<sub>3</sub> concentration at XJH and PD increases more rapidly than that  
683 in daytime response the NO<sub>x</sub> reduction.

684 (3) The WRF-Chem model is utilized to calculate the long term O<sub>3</sub> variations response to  
685 emission change. The sensitive experiments illustrate that either reduction of NO<sub>x</sub> emission or  
686 growth of VOCs emission conducted by WRF-Chem lead to the significant enhancement in O<sub>3</sub>  
687 concentration in urban zones in 2009 as the baseline, indicating the O<sub>3</sub> production is clearly  
688 under VOC-limited regime. The calculated O<sub>3</sub> concentration increases by 1-7 ppbv in urban zones  
689 from 2009 to 2015 resulted from 30% reduction of NO<sub>x</sub> emission estimated by Shanghai  
690 Environmental Monitoring Center. The enhancement of O<sub>3</sub> concentration is significant in urban  
691 zones generally more than 4 ppbv, with the maximum elevation of 6-7 ppbv occurred at  
692 downtown area, which is consistent with the measurements. The increasing rates of O<sub>3</sub> trend at  
693 downtown site XJH and sub-urban site PD are estimated at 1.06 ppbv yr<sup>-1</sup> and 0.96 ppbv yr<sup>-1</sup> from  
694 2009 to 2015 by WRF-Chem, which is close to the observed O<sub>3</sub> growth variability of 1-1.3 ppbv  
695 yr<sup>-1</sup>. This result suggests that the observed increasing trend of O<sub>3</sub> concentration during the past  
696 ten years in Shanghai is likely attributed to the reduction of NO<sub>x</sub> emission under the VOC-limited  
697 condition for O<sub>3</sub> production.

698 (4) The model sensitive study suggests that significant decrease in NO<sub>x</sub> concentration  
699 combined with the obscure VOCs variation from 2006 to 2015 gradually promotes the O<sub>3</sub>  
700 chemical production in Shanghai from VOC-limited to NO<sub>x</sub>-limited, which is consistent with the O<sub>3</sub>  
701 isopleths diagram. The O<sub>3</sub> isopleths plot shows that O<sub>3</sub> production is in VOC-limited regime in  
702 both downtown site XJH and sub-urban site PD in 2009. With the 30% reduction of NO<sub>x</sub> emission



---

703 from 2009 to 2015 estimated by Shanghai Environmental Monitoring Center, the O<sub>3</sub> production in  
704 XJH is still under VOC-limited regime, while the O<sub>3</sub> production moves to the transition regime in  
705 PD, suggesting that the O<sub>3</sub> concentration in sub-urban zones is not sensitive to the variation of  
706 either NO<sub>x</sub> or VOCs concentration.

707 (5) In order to better understand the O<sub>3</sub> control strategy in Shanghai, the future O<sub>3</sub>  
708 production is estimated by WRF-Chem. The O<sub>3</sub> concentration in Shanghai downtown would keep  
709 increasing till 2020 with the 20% reduction of NO<sub>x</sub> emission after 2015 estimated by Shanghai  
710 Clean Air Action Plan. If the NO<sub>x</sub> emission is further decreased by 20% after 2020, The O<sub>3</sub>  
711 concentration will decrease by 2-3 ppbv in sub-urban zones, and more than 4 ppbv in suburb.  
712 While the O<sub>3</sub> concentration in downtown is not sensitive to either NO<sub>x</sub> reduction or VOCs  
713 enhancement after 2020, indicating the O<sub>3</sub> production in shanghai will transfer to NO<sub>x</sub>-limited  
714 regimes except downtown where the O<sub>3</sub> production is likely close to the transition regime.  
715 Further reduction of NO<sub>x</sub> emission after 2020 tend to mitigate the O<sub>3</sub> pollution in Shanghai.

716

717

718 **Data availability.** The data used in this paper can be provided upon request from Jianming Xu  
719 (metxujm@163.com).

720

721 **Author contributions.** XT came up with the original idea of investigating the impact of emission  
722 change on long term O<sub>3</sub> variations by. XT and JX designed the analysis method. JX conducted the  
723 analysis. WG, YL and QF provided the observational data and helped in discussion.

724

725 **Competing interests.** The authors declare that they have no conflict of interest.

726

727 **Acknowledgements.** This study was funded by the National Key R&D Program of China (grant  
728 2018YFC0213800), the National Natural Science Foundation of China (91644223, 41430424 and  
729 41730108).

730

731 **References**

- 732 Binkowski, F. S. and Roselle, S. J.: Models-3 community multi scale air quality (CMAQ) model  
733 aerosol component – 1. Model description, *Journal of Geophysical Research*, 108 (D6),  
734 4183, doi:10.1029/2001jd001409, 2003.
- 735 Brasseur, G. P., Orlando, J. J., and Tyndall, G. S.: *Atmospheric chemistry and global change*, Oxford  
736 University Press, Cambridge, USA, 654 pp., 1999.
- 737 Cai, C. J., Geng, F. H., Tie, X. X., Yu, Q., and An J. L.: Characteristics and source apportionment of  
738 VOCs measured in Shanghai, China, *Atmospheric Environment*, 44, 5005-5014, 2010.
- 739 Chen, F. and Dudhia, J.: Coupling an advanced land surface hydrology model with the Penn  
740 State-NCAR MM5 modeling system, Part I: Model implementation and sensitivity, *Monthly  
741 Weather Review*, 129, 569–585, 2001.
- 742 Dudhia, J.: Numerical study of convection observed during the winter monsoon experiment using  
743 a mesoscale two-dimensional model, *Journal of the Atmospheric Sciences*, 46, 3077–3107,  
744 1989.
- 745 Emmons, L. K., Walters, S., Hess, P. G., Lamarque, J. F., Pfister, G. G., Fillmore, D., Granier, C.,  
746 Aguenther, A., Kinnison, D., Laepple, T., Orlando, J., Tie, X., Tyndall, G., Wiedinmyer, C.,  
747 Baughcum, S. L., and Kloster, S.: Description and evaluation of the model for ozone and  
748 related chemical tracers, version4 (MOZART-4), *Geoscientific Model Development*, 3, 43–67,  
749 2010.
- 750 Gao, W., Tie, X. X., Xu, J. M., Huang, R. J., Mao, X. Q., Zhou, G. Q., and Chang, L. Y.: Long-term  
751 trend of O<sub>3</sub> in a mega City (Shanghai), China: Characteristics, causes, and interactions with  
752 precursors, *Science of the Total Environment*, 603-604, 425-433, 2017.
- 753 Geng, F. H., Zhao, C. S., Tang, X., Lu, G. L., and Tie, X. X.: Analysis of ozone and VOCs measured in  
754 Shanghai: a case study, *Atmospheric Environment*, 41, 989–1001, 2007.
- 755 Geng, F. H., Tie, X., Xu, J., Zhou, G., Peng, L., Gao, W., Tang, X., Zhao, C.: Characterizations of ozone,  
756 NO<sub>x</sub>, and VOCs measured in Shanghai, China, *Atmospheric Environment*, 42, 6873–6883,  
757 2008a.
- 758 Geng, F. H., Zhang, Q., Tie, X., Huang, M., Ma, X., Deng, Z., Quan, J., and Zhao, C.: Aircraft  
759 measurements of O<sub>3</sub>, NO<sub>x</sub>, CO, VOCs, and SO<sub>2</sub> in the Yangtze River Delta region, *Atmospheric  
760 Environment*, 43, 584–593, 2008b.
- 761 Geng, F. H., Tie, X., Guenther, A., Li, G., Cao, J., and Harley, P.: Effect of isoprene emissions from  
762 major forests on ozone formation in the city of Shanghai, China, *Atmospheric Chemistry and  
763 Physics*, 11, 10449–10459, 2011.
- 764 Geng, F. H., Mao, X. Q., Zhou, M. Y., Zhong, S. Y., and Lenschow, D.: Multi-year ozone  
765 concentration and its spectra in Shanghai, China, *Science of the Total Environment*, 521-522,  
766 135-143, 2015.
- 767 Gery, M. W., and Crouse, R. R.: *User's Guide for Executing OZIPR*, Atmospheric Research and  
768 Exposure Assessment Lab., Office of Research and Development, U.S. EPA, Research Triangle  
769 Park, N. C., <http://www.epa.gov/scram001/models/other/oziprdme.txt>, 2002.
- 770 Grell, G. A., Peckham, S. E., Schmitz, R., McKeen, S. A., Frost, G., Skamarock, W. C., and Eder, B.:  
771 Fully coupled “online” chemistry within the WRF model, *Atmospheric Environment*, 39,  
772 6957–6975, 2005.
- 773 Guenther, A., Karl, T., Harley, P., Wiedinmyer, C., Palmer, P. I., and Geron, C.: Estimates of global  
774 terrestrial isoprene emissions using MEGAN (Model of Emissions of Gases and Aerosols from



- 775 Nature), *Atmospheric Chemistry and Physics*, 6, 3181–3210, 2006.
- 776 Hong, S. Y. and Lim, J. O. J.: The WRF Single-Moment 6-Class Microphysics Scheme (WSM6),  
777 *Journal of the Korean Meteorological Society*, 42, 129–151, 2006.
- 778 Lei, W., Foy, B. de, Zavala, M., Volkamer, R., and Molina, L. T.: Characterizing ozone production in  
779 the Mexico City Metropolitan Area: a case study using a chemical transport model,  
780 *Atmospheric Chemistry and Physics*, 7, 1347–1366, 2007.
- 781 Li, G., Lei, W., Zavala, M., Volkamer, R., Dusanter, S., Stevens, P., and Molina, L. T.: Impacts of  
782 HONO sources on the photochemistry in Mexico City during the MCMA-2006/MILAGO  
783 Campaign, *Atmospheric Chemistry and Physics*, 10, 6551–6567, 2010.
- 784 Li, G., Bei, N., Tie, X., and Molina, L. T.: Aerosol effects on the photochemistry in Mexico City  
785 during MCMA-2006/MILAGRO campaign, *Atmospheric Chemistry and Physics*, 11,  
786 5169–5182, 2011.
- 787 Li, K., Jacob, D. J., Liao, H., Shen, L., Zhang, Q., and Bates, K. H.: Anthropogenic drivers of  
788 2013–2017 trends in summer surface ozone in China, *PANS*, 116, 2, 422–427, 2019.
- 789 Lin, X., Trainer, M., and Liu, S. C.: On the nonlinearity of the tropospheric ozone production,  
790 *Journal of Geophysical Research Atmospheres*, 93 (D12), 15879–15888, 1988.
- 791 Lin, Y. F., Wang, Q., Fu, Q. Y., Duan, Y. S., Xu, J. M., Liu, Q. Z., Li, F., and Huang, K.: Temporal-spatial  
792 characteristics and impact factors of ozone pollution in Shanghai, *Environmental Monitoring*  
793 *in China (in Chinese)*, 33, 4, 60–67, 2017.
- 794 Lin, Y. L., Farley, R. D., and Orville, H. D.: Bulk parameterization of the snowfield in a cloud model,  
795 *Journal of Climate and Applied Meteorology*, 22, 1065–1092, 1983.
- 796 Lu, X., Hong, J., Zhang, L., Cooper, O., Schultz, M., Xu, X., Wang, T., Gao, M., Zhao, Y., and Zhang, Y.:  
797 Severe surface ozone pollution in China: A global perspective, *Environmental Science*  
798 *& Technology Letters*, 5, 487–494, 2018.
- 799 Monks, P. S., Archibald, A. T., Colette, A., Cooper, O., Coyle, M., Derwent, R., Fowler, D., Granier, C.,  
800 Law, K. S., Mills, G. E., Stevenson, D. S., Tarasova, O., Thouret, V., von Schneidmesser, E.,  
801 Sommariva, R., Wild, O., and Williams, M. L.: Tropospheric ozone and its precursors from the  
802 urban to the global scale from air quality to short-lived climate forcer, *Atmospheric*  
803 *Chemistry and Physics*, 15, 8889–8973, 2015.
- 804 Ma, Z., Xu, J., Quan, W., Zhang, Z., Lin, W., and Xu, X.: Significant increase of surface ozone at a  
805 rural site, north of eastern China, *Atmospheric Chemistry and Physics*, 16, 3969–3977, 2016.
- 806 Nenes, A., Pandis, S. N., and Pilinis, C.: ISORROPIA: A new thermodynamic equilibrium model for  
807 multiphase multicomponent inorganic aerosols, *Aquatic Geochemistry*, 4, 123–152, 1998.
- 808 Ran, L., Zhao, C., Geng, F., Tie, X., Tang, X., Peng, L., Zhou, G., Yu, Q., Xu, J., and Guenther, A.:  
809 Ozone photochemical production in urban Shanghai, China: analysis based on ground level  
810 observations, *Journal of Geophysical Research Atmospheres*, 114, D15301, 2009.
- 811 Sillman, S.: The use of NO<sub>y</sub>, H<sub>2</sub>O<sub>2</sub>, and HNO<sub>3</sub> as indicators for ozone-NO<sub>x</sub>-hydrocarbon sensitivity  
812 in urban locations, *Journal of Geophysical Research Atmospheres*, 100, 14175–14188, 1995.
- 813 Sillman, S.: The relation between ozone, NO<sub>x</sub> and hydrocarbons in urban and polluted rural  
814 environments, *Atmospheric Environment*, 33, 1821–1845, 1999.
- 815 Song, J., Lei, W., Bai, N., Zavala, M., de Foy, B., Volkamer, R., Cardenas, B., Zheng, J., Zhang, R., and  
816 Molina L. T.: Ozone response to emission changes: a modeling study during the  
817 MCMA-2006/MILAGRO Campaign, *Atmospheric Chemistry and Physics*, 10, 3827–3846, 2010
- 818 Stockwell, W. R., Middleton, P., Chang, J. S., and Tang, X.: The second generation regional acid



- 819 deposition model chemical mechanism for regional air quality modeling, *Journal of*  
820 *Geophysical Research Atmospheres*, 95, 16343–16367, 1990.
- 821 Sun, L., Xue, L., Wang, T., Gao, J., Ding, A., Copper, O., Lin, M., Xu, P., Wang, Z., Wang, X., Wen, L.,  
822 Zhu, Y., Chen, T., Yang, L., Wang, Y., Chen, J., and Wang, W.: Significant increase of  
823 summertime ozone at Mount Tai in central eastern China, *Atmospheric Chemistry and*  
824 *Physics*, 16, 10637–10650, 2016.
- 825 Tai, A. P. K., Martin, M. V., and Heald, C. L.: Threat to future global food security from climate  
826 change and ozone air pollution, *Nature Climate Chang*, 4, 817–821, 2014.
- 827 Tang, G., Li, X., Wang, Y., Xin, J., and Ren, X.: Surface ozone trend details and interpretations in  
828 Beijing, 2001–2006, *Atmospheric Chemistry and Physics*, 9, 8813–8823, 2009.
- 829 Tang, W. Y., Zhao, C. S., Geng, F. H., Peng, L., Zhou, G. Q., Gao, W., Xu, J. M., and Tie, X. X.: Study of  
830 ozone "weekend effect" in Shanghai, *Science in China Series D: Earth Sciences*, 51, 9,  
831 1354–1360, 2008.
- 832 Tie, X., Brasseur, G., Emmons, L., Horowitz, I., and Kinnison, D.: Effects of aerosols on  
833 tropospheric oxidants: a global model study, *Journal of Geophysical Research Atmospheres*,  
834 106, 22931–22964, 2001.
- 835 Tie, X., Madronich, S., Walters, S., Zhang, R. Y., Rasch, P., and Collins, W.: Effect of clouds on  
836 photolysis and oxidants in the troposphere, *Journal of Geophysical Research Atmospheres*,  
837 108, 4642, doi:10.1029/2003jd003659, 2003.
- 838 Tie, X., Madronich, S., Li, G., Ying, Z., Zhang, R., Garcia, A., Taylor, J., and Liu, Y.: Characterizations  
839 of chemical oxidants in Mexico City: A regional chemical dynamical model (WRF-Chem)  
840 study, *Atmospheric Environment*, 41, 1989–2008, 2007.
- 841 Tie, X., Geng, F. H., Peng, L., Gao, W., Zhao, C. S.: Measurement and modeling of O<sub>3</sub> variability in  
842 Shanghai, China: application of the WRF-Chem model, *Atmospheric Environment*, 43,  
843 4289–4302, 2009a.
- 844 Tie, X., Madronich, S., Li, G., Ying, Z., Weinheimer, A., Apel, E., and Campos, T.: Simulation of  
845 Mexico City plumes during the MIRAGE-Mex field campaign using the WRF-Chem model,  
846 *Atmospheric Chemistry and Physics*, 9, 4621–4638, 2009b.
- 847 Tie, X., Geng, F., Guenther, A., Cao, J., Greenberg, J., Zhang, R., Apel, E., Li, G., Weinheimer, A.,  
848 Chen, J., and Cai, C.: Megacity impacts on regional ozone formation: observations and  
849 WRF-Chem modeling for the MIRAGE-Shanghai field campaign, *Atmospheric Chemistry and*  
850 *Physics*, 13, 5655–5669, doi:10.5194/acp-13-5655-2013, 2013.
- 851 Wang, H. J., and Chen, H. P.: Understanding the recent trend of haze pollution in eastern China:  
852 roles of climate change, *Atmospheric Chemistry and Physics*, 16, 4205–4211, 2016
- 853 Wang, T., Xue, L., Brimblecombe, P., Lam Y. F., Li, L., and Zhang, L.: Ozone pollution in China: A  
854 review of concentrations, meteorological influences, chemical precursors, and effects,  
855 *Science of Total Environment*, 575, 1582–1596, 2017.
- 856 Wesely, M. L.: Parameterization of surface resistances to gaseous dry deposition in regional-scale  
857 numerical models, *Atmospheric Environment*, 23, 1293–1304, 1989.
- 858 Xu, J. M., Yan, F. X., Xie, Y., Wang, F. Y., Wu, J. B., and Fu, Q. Y.: Impact of meteorological conditions  
859 on a nine-day particulate matter pollution event observed in December 2013, Shanghai,  
860 China, *Particuology*, 20, 69–79, 2015.
- 861 Xu, J. M., Chang, L. Y., Yan, F. X., and He, J. H.: Role of climate anomalies on decadal variation in  
862 the occurrence of wintertime haze in the Yangtze River Delta, China, *Science of the Total*



- 
- 863 Environment, 599-600, 918-925, 2017.
- 864 Ying, Z. M., Tie, X., and Li, G. H.: Sensitivity of ozone concentrations to diurnal variations of  
865 surface emissions in Mexico City: A WRF/Chem modeling study, Atmospheric Environment,  
866 43, 851–859, 2009.
- 867 Zhang, Q., Streets, D. G., Carmichael, G. R., He, K. B., Huo, H., Kannari, A., Klimont, Z., Park, I. S.,  
868 Reddy, S., Fu, J. S., Chen, D., Duan, L., Lei, Y., Wang, L. T., Yao, Z. L.: Asian emissions in 2006  
869 for the NASA INTEX-B mission, Atmospheric Chemistry and Physics, 9, 5131-5153, 2009.
- 870 Zhao, S., Li, J. P., Sun, C.: Decadal variability in the occurrence of wintertime haze in central  
871 eastern China tied to the Pacific decadal oscillation, Scientific Reports, 6, 27424, 2016.
- 872 Zheng, B., Tong, D., Li, M., Liu, F., Hong, C., Geng, G., Li, H., Li, X., Peng, L., Qi, J., Yan, L., Zhang, Y.,  
873 Zhao, H., Zheng, Y., He, K., and Zhang, Q.: Trends in China's anthropogenic emissions since  
874 2010 as the consequence of clean air actions, Atmospheric Chemistry and Physics, 18,  
875 14095-14111, <https://doi.org/10.5194/acp-18-14095-2018>, 2018.
- 876 Zhou, G. Q., Xu, J. M., Xie, Y., Chang, L. Y., and Gao, W.: Numerical air quality forecasting over  
877 eastern China: An operational application of WRF-Chem, Atmospheric Environment, 153,  
878 94-108, 2017.
- 879





880 **Table 1.** Statistical analysis on O<sub>3</sub> simulation in September of 2009 by WRF-Chem model  
881 compared with measurements of 5 sites (XJH, JS, DT, PD, BS) over Shanghai. MO and MM  
882 represent the mean value (unit: ppbv) of observed and modeled O<sub>3</sub> concentration respectively.  
883 RMSE and R are the Root Mean Square Error and correlated coefficient respectively calculated  
884 between modeled and measured O<sub>3</sub> concentration.

885

	MO	MM	RMSE	R (99% confidence)
		ppbv		\
<b>XJH</b>	21.6	23.0	7.2	0.78
<b>JS</b>	34.6	30.0	10.3	0.64
<b>DT</b>	47.3	40.3	12.0	0.61
<b>PD</b>	33.5	34.9	8.6	0.74
<b>BS</b>	31.7	31.2	9.3	0.67

886

887

888

889 **Table 2.** Statistical analysis on NO<sub>x</sub> simulation in September of 2009 by WRF-Chem model  
890 compared with measurements of 5 sites (XJH, JS, DT, PD, BS) over Shanghai. MO and MM  
891 represent the mean value (unit: ppbv) of observed and modeled NO<sub>x</sub> concentration respectively.  
892 RMSE and R are the Root Mean Square Error and correlated coefficient respectively calculated  
893 between modeled and measured NO<sub>x</sub> concentration.

894

	MO	MM	RMSE	R (99% confidence)
		ppbv		\
<b>XJH</b>	32.1	33.7	7.0	0.74
<b>JS</b>	14.9	14.7	7.6	0.61
<b>DT</b>	3.0	1.5	2.3	0.6
<b>PD</b>	20.3	16.8	7.5	0.82
<b>BS</b>	21.6	16.1	9.8	0.8

895

896

897 **Table 3.** Scheme of WRF-Chem sensitivity simulations.

898

Simulation	NO <sub>x</sub> EI	VOCs EI	Meteorology
<b>T1 (Control Run)</b>	2009	2009	September of 2009
<b>T2</b>	2015 (30% reduction)	2009	September of 2009
<b>T3</b>	2009	50% increasing	September of 2009
<b>T4</b>	2020 (50% reduction)	2009	September of 2009
<b>T5</b>	2015	50% increasing	September of 2009
<b>T6</b>	70% reduction	2009	September of 2009
<b>T7</b>	2020 (50% reduction)	50% increasing	September of 2009

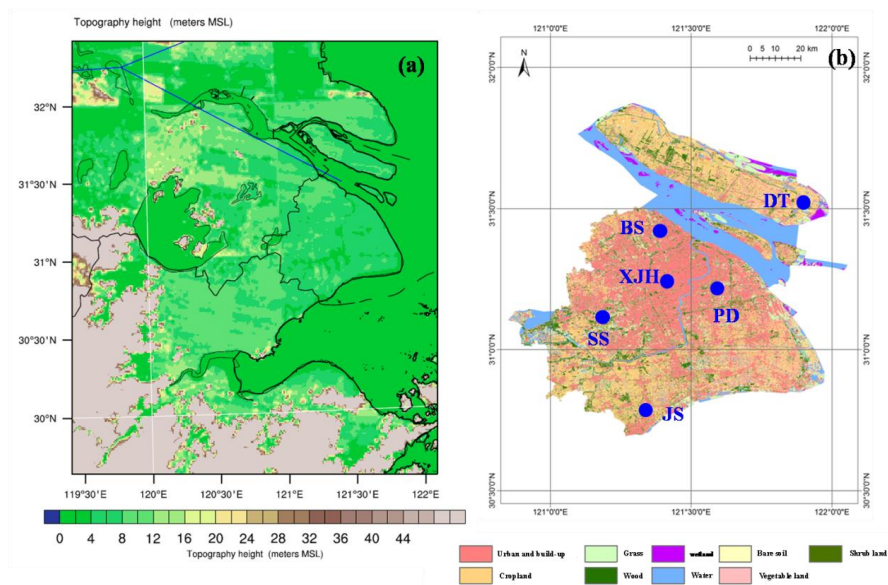
899

900

901



902



903

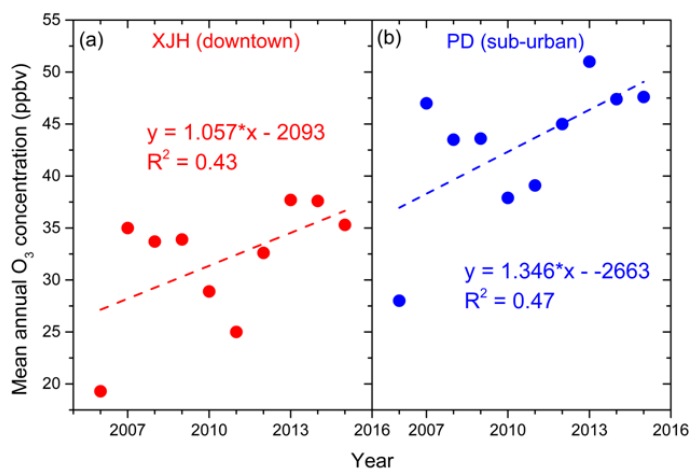
904

905

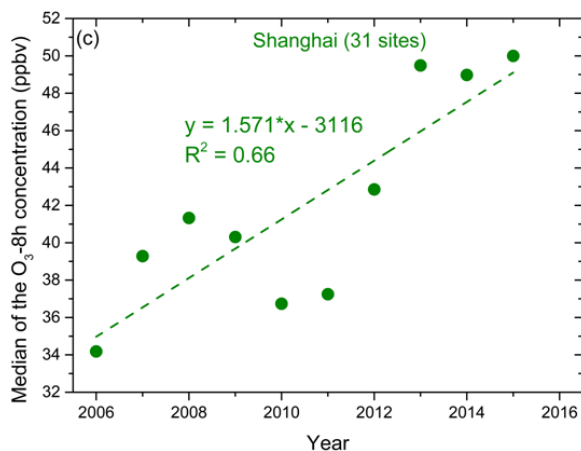
906

907

**Figure 1.** (a) The distribution of topography height in Shanghai and its neighboring area. (b) The distribution of land-use category in Shanghai. The locations of the 6 sites (XJH, BS, PD, SS, JS, DT) are described by blue dots.

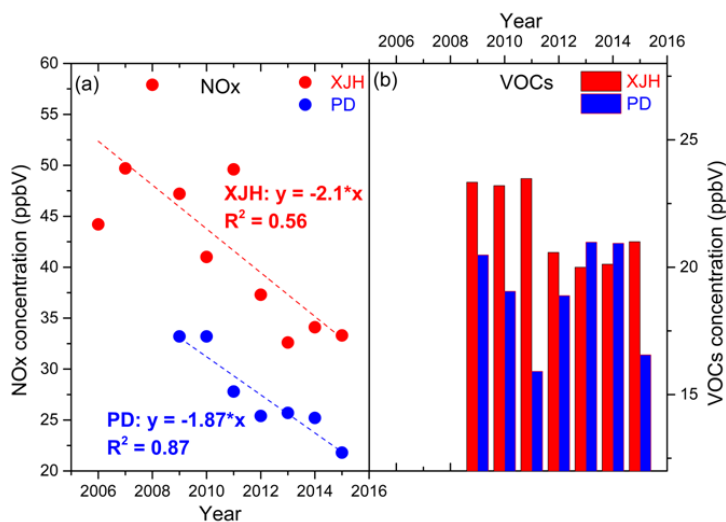


908



909

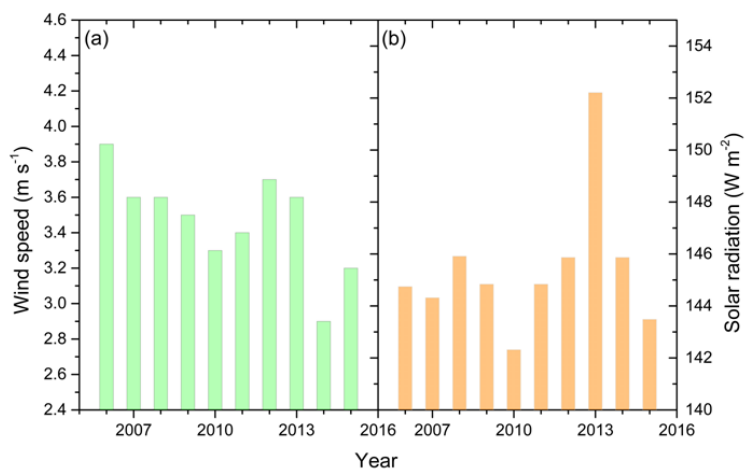
910 **Figure 2.** The mean annual O<sub>3</sub> concentration (ppbv) from 2006 to 2015 at (a) downtown site XJH  
911 and (b) sub-urban site PD, both presenting the significant increasing trends with 1.057 ppbv yr<sup>-1</sup>  
912 at XJH and 1.346 ppbv yr<sup>-1</sup> at PD. The variation of the median 8-h O<sub>3</sub> concentration (ppbv) from  
913 2006 to 2015 averaged for 31 sites over Shanghai (c), also shows the increasing variability of  
914 1.571 ppbv yr<sup>-1</sup>.



915

916 **Figure 3.** The mean annual concentrations (ppbv) of (a) NO<sub>x</sub> (dots) and (b) VOCs (bars) from 2006  
917 to 2015 at downtown site XJH and sub-urban site PD respectively. The NO<sub>x</sub> concentrations at XJH  
918 and PD both present obvious decreasing trends with 2.1 ppbv yr<sup>-1</sup> and 1.87 ppbv yr<sup>-1</sup>. While the  
919 VOCs concentrations at both sites present no clear inter-annual trends.

920



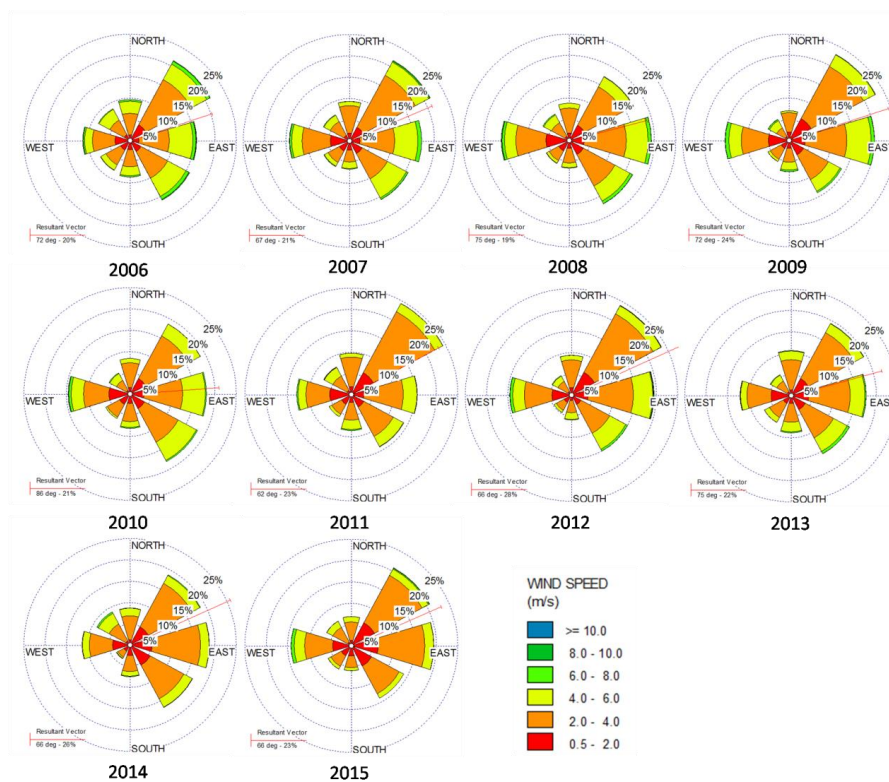
921

922 **Figure 4.** The annual variation of (a) summer wind speed ( $\text{m s}^{-1}$ ) and (b) total solar radiation ( $\text{W}$   
923  $\text{m}^{-2}$ ) from 2006 to 2015 in Shanghai. Both wind speed and the solar radiation present weak  
924 inter-annual variations but without significant trends.

925

926

927



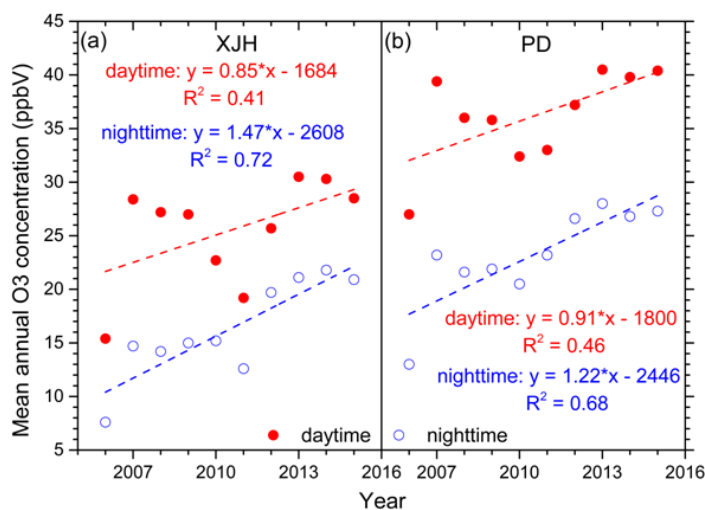
928

929 **Figure 5.** The wind rose of each year from 2006 to 2015 in Shanghai. The red line means the  
930 resultant vector suggesting the dominant wind direction.

931

932

933

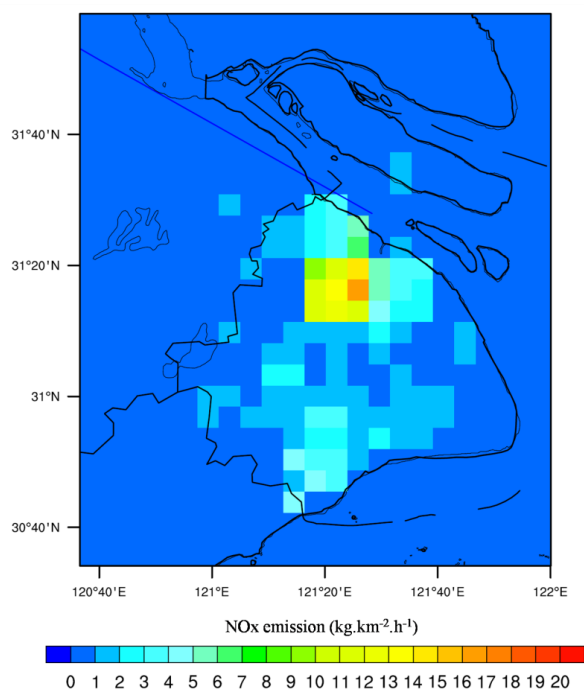


934

935 **Figure 6.** The annual variations of daytime and nighttime O<sub>3</sub> concentration (ppbv) from 2006 to  
936 2015 at (a) downtown site XJH and (b) sub-urban site PD.

937

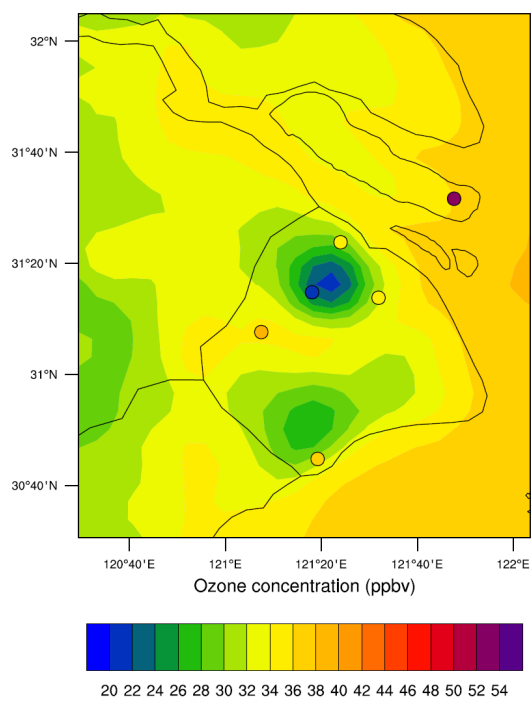
938



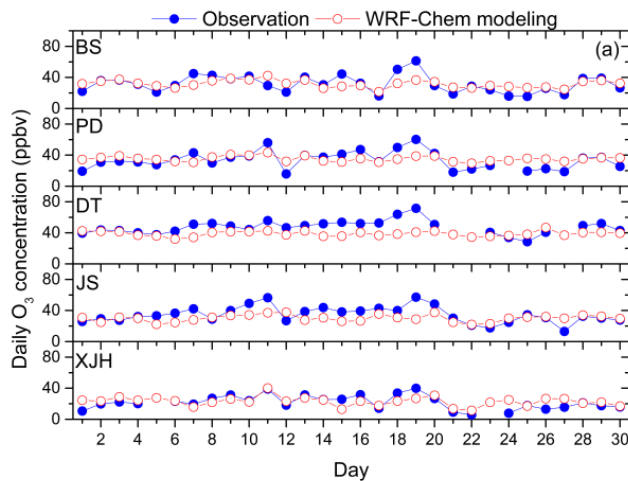
939

940 **Figure 7.** The distribution of NO<sub>x</sub> emission (kg km<sup>-2</sup> h<sup>-1</sup>) in 2009 in Shanghai.

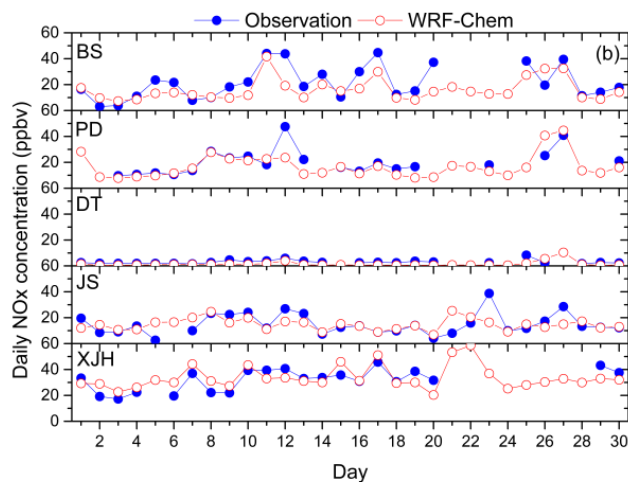




941  
942 **Figure 8.** The calculated distribution of O<sub>3</sub> concentration by WRF-Chem (shade) in September of  
943 2009 compared with measurements (circles) of 6 sites over Shanghai.  
944

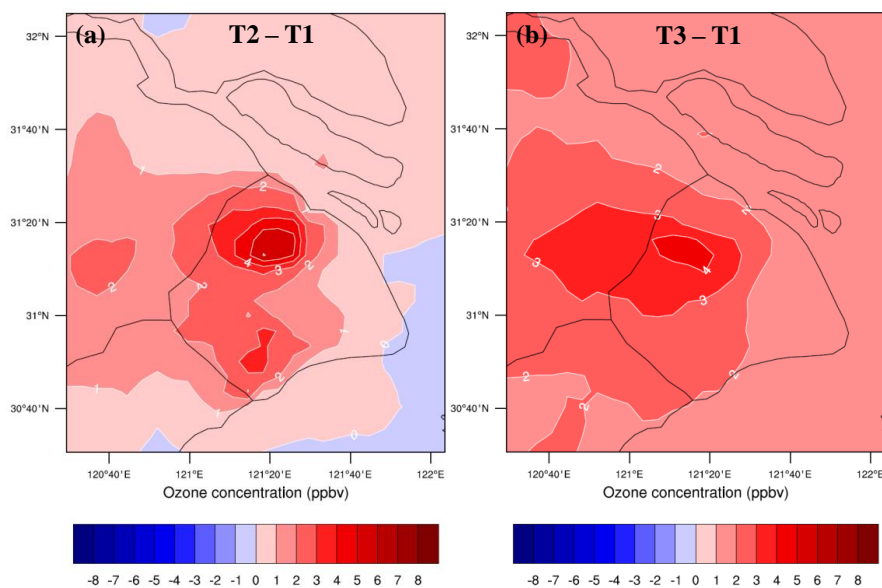


945



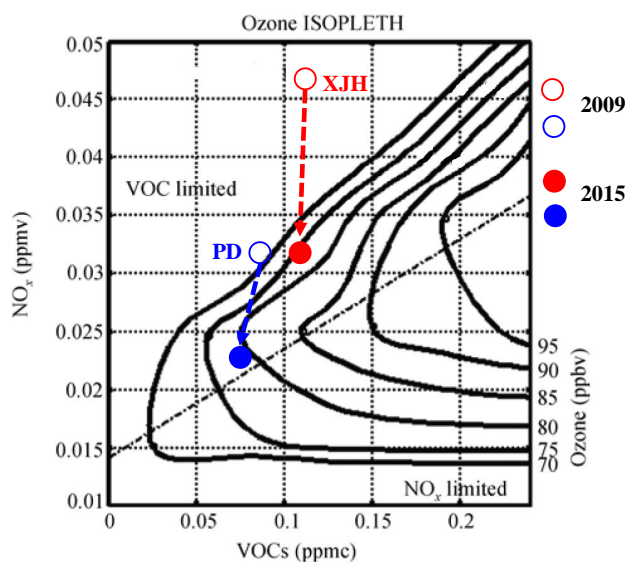
946

947 **Figure 9.** The calculated mean daily concentrations (ppbv) of (a) O<sub>3</sub> and (b) NO<sub>x</sub> at 5 sites in  
948 September of 2009 by WRF-Chem (red circles) and compared with measurements (blue circles).  
949



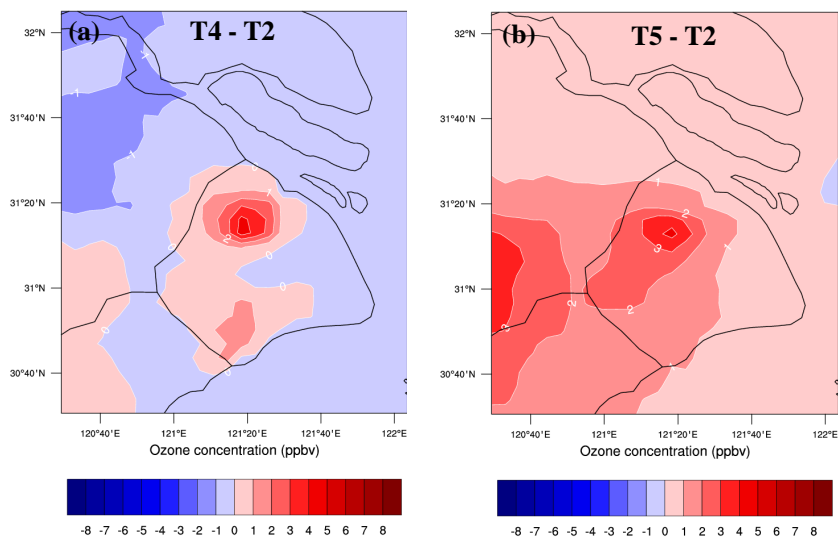
950

951 **Figure 10.** The difference of O<sub>3</sub> concentration (ppbv) between (a) T2 and T1 (T2-T1), (b) T3 and  
 952 T1 (T3-T1) respectively conducted by WRF-Chem model. The difference between T2 and T1 lies in  
 953 the NO<sub>x</sub> emissions set in T2 (2015 scenario) is 30% lower than that in T1 (2009 scenario), which is  
 954 estimated by Lin et al. (2017) according to the Shanghai Environment Yearbook. The difference  
 955 between T3 and T1 is dependent on that the VOCs emission in T3 is 50% higher than that in T1.

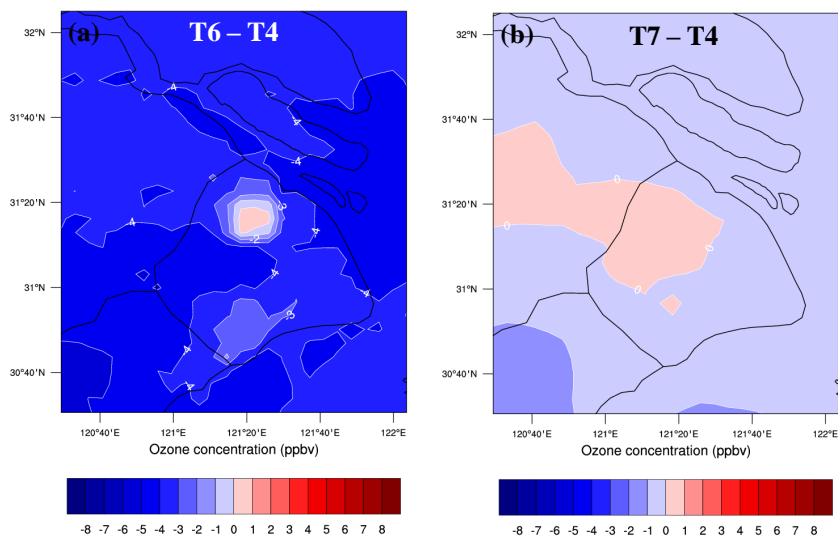


956

957 **Figure 11.** The O<sub>3</sub> chemical production at downtown site XJH and sub-urban site PD in 2009 and  
 958 2015 depicted by O<sub>3</sub> isopleths diagram. The hollow and solid red circles denote O<sub>3</sub> production  
 959 regime at XJH in 2005 and 2019 respectively. The hollow and solid blue circles denote O<sub>3</sub>  
 960 production regime at PD in 2005 and 2019 respectively



961  
 962 **Figure 12.** The difference of O<sub>3</sub> concentration (ppbv) between (a) T4 and T2 (T4-T2), (b) T5 and  
 963 T2 (T5-T2) respectively conducted by WRF-Chem model. The difference between T4 and T2 is  
 964 that the NO<sub>x</sub> emissions set in T4 (2020 scenario) is 20% lower than that in T2 (2015 scenario),  
 965 which is estimated according to the Shanghai Clean Air Action Plan. The difference between T5  
 966 and T2 lies in that the VOCs emission in T5 is 50% higher than that in T2.  
 967  
 968  
 969  
 970



971  
972 **Figure 13.** The difference of O<sub>3</sub> concentration (ppbv) between (a) T6 and T4 (T6-T4), (b) T7 and  
973 T4 (T7-T4) respectively conducted by WRF-Chem model. The NO<sub>x</sub> emissions set in T6 is 20% lower  
974 than that in T4 (2020 scenario). The VOCs emission in T7 is 50% higher than that in T4.